The Smithian–Spathian boundary in North Greenland: implications for extreme global climate changes

Sofie Lindström[1],* , Morten Bjerager[1] , Peter Alsen[1] , Hamed Sanei[2] and Jørgen Bojesen-Koefoed[1]

[1]Geological Survey of Denmark and Greenland, Øster Voldgade 10, DK-1350 Copenhagen K, Denmark and [2]Department of Geoscience, Aarhus University, Høegh-Guldbergs Gade 2, DK-8000 Aarhus, Denmark

Abstract

Smithian–lower Anisian strata in Peary Land, North Greenland, were deposited at ~45° N on the northern margin of Pangaea in offshore to upper shoreface settings. The well-constrained succession (palynology and ammonite biostratigraphy) documents a remarkable shift from lycophyte spore-dominated assemblages in the upper Smithian to gymnosperm pollen-dominated ones in the lower Spathian in concert with a marked shift of +6 ‰ in $\delta^{13}C_{org}$. Correlation with other Smithian–Spathian boundary sections that record terrestrial floral changes indicates that the recovery of gymnosperms began earlier in the mid-latitudes of the Southern Hemisphere than in the Northern Hemisphere. The lycophyte-dominated Late Smithian Thermal Maximum is here interpreted as reflecting dry and hot climatic conditions with only brief seasonal precipitation unable to sustain large areas of gymnosperm trees, but able to revive dehydrated lycophytes. This suggests that the Late Smithian Thermal Maximum was a time of widespread aridity, which is also supported by red bed deposition in many areas globally, even as far south as Antarctica. The shift to gymnosperm-dominated vegetation during the cooling across the Smithian–Spathian boundary reflects a change to seasonally more humid climatic conditions favouring gymnosperm recovery, and could have been initiated by increased albedo over land due to the widespread aridity during the Late Smithian Thermal Maximum. The recovery of gymnosperm vegetation would have helped to draw down CO_2 from the atmosphere and exacerbate global cooling.

1. Introduction

In the aftermath of the end-Permian mass extinction, the Early Triassic period (~252 to ~247 Ma) was an interval of delayed biotic recovery both in the oceans and on land (Looy *et al.* 1999; Payne *et al.* 2004; Chen & Benton, 2012; Hochuli *et al.* 2016). Episodes of partial recovery during Early Triassic time were cut short by minor marine extinction events in early Griesbachian time, at the Griesbachian–Dienerian boundary and at the Smithian–Spathian boundary (SSB) (Sun *et al.* 2012; Romano *et al.* 2013), as well as marked changes in the terrestrial vegetation record (Galfetti *et al.* 2007*b*; Hochuli *et al.* 2016). These events were most likely linked to extreme global warming, resulting in lethally hot conditions, with tropical sea surface temperatures >35 °C, resulting in widespread euxinia in the oceans (Sun *et al.* 2012). Highly fluctuating C-isotope records testify to rapid and large-scale perturbations in the carbon cycle (Payne *et al.* 2004). It is suggested that full recovery of the marine ecosystem first occurred during Middle Triassic time (Chen & Benton, 2012).

Similarly, terrestrial plants were severely affected during the end-Permian event, with taxonomic losses but, perhaps more importantly, major restructuring of the terrestrial plant communities (Lindström & McLoughlin, 2007; Hermann *et al.* 2012*b*; Hochuli *et al.* 2016). Recovery on land was originally believed to have been delayed worldwide until early Anisian time (Looy *et al.* 1999), resulting in a marked global coal gap (Retallack *et al.* 1996). However, later research has shown that the composition of the terrestrial ecosystem has fluctuated between floras dominated by spore-producing plants and those dominated by gymnosperms (Looy *et al.* 1999; Schneebeli-Hermann *et al.* 2015, 2017; Hochuli *et al.* 2016).

The late Smithian was one of the hottest intervals during Early Triassic time, with extreme temperatures both in the upper tropical ocean and on land (Sun *et al.* 2012). This is reflected by a pronounced negative $\delta^{13}C$ excursion (CIE), with a magnitude of ~6 ‰, in both carbonate and organic material (Payne *et al.* 2004; Galfetti *et al.* 2007*b*; Tong *et al.* 2007; Horacek *et al.* 2009; Hermann *et al.* 2011; Clarkson *et al.* 2013; Grasby *et al.* 2013*a*,*b*; Wignall *et al.* 2016; Komatsu *et al.* 2016). During this Late Smithian Thermal Maximum (LSTM), upper water column temperatures at equatorial latitudes are estimated to have approached 38 °C, with sea surface temperature possibly exceeding 40 °C, as inferred from oxygen isotope ratios of conodont apatite (Sun *et al.* 2012). The LSTM is succeeded by a relatively sharp positive C-isotope excursion of

similar magnitude at the SSB, which has been attributed to a strong cooling of the tropical sea surface, as oxygen isotopes from conodont apatite indicate an almost 5 °C cooling of the upper water column in the equatorial ocean (Sun et al. 2012; Romano et al. 2013). The SSB is marked by extinctions amongst nektonic organisms, with severe losses amongst conodonts and ammonoids (Orchard, 2007; Brayard et al. 2006, 2009; Stanley, 2009). Faunal losses amongst benthic organisms included many so-called disaster taxa that had proliferated in the aftermath of the end-Permian crisis, e.g. bellerophontid gastropods and bivalves (Kaim & Nutzel, 2011; Sun et al. 2015). Several models have been invoked to explain these major perturbations of the carbon cycle. Payne et al. (2004) suggested that the pronounced negative excursion in the Smithian was caused by injection of isotopically light carbon from volcanic activity in the Siberian Traps large igneous province. Such a scenario could explain records indicating global warming and ocean anoxia, followed by enhanced carbon burial resulting in global cooling as reflected in a positive excursion at the SSB (Galfetti et al. 2007a, 2008; Saito et al. 2013). This hypothesis is possibly supported by an increase in mercury content and the Hg/TOC (total organic carbon) ratio during the Smithian in the Sverdrup Basin, Arctic Canada, and on Svalbard (Grasby et al. 2013b, 2016). Payne et al. (2004) further found a methane-driven scenario for the highly fluctuating Early Triassic carbon cycle unlikely. They estimated that more than 10000 Gt of methane, five times the amount estimated for the Paleocene–Eocene Thermal Maximum (Dickens et al. 1995), would have been required to produce the ∼8 ‰ drop over 100 to 500 kyrs from the late Dienerian to Smithian. They instead favoured massive changes in organic carbon burial relative to carbonate carbon, with episodes of extraordinarily high organic carbon burial alternated with intervals with much lower fractionation of organic carbon burial (Payne et al. 2004). However, other authors have suggested alternative scenarios to the carbon cycle perturbations. Horacek et al. (2007) argued that the Smithian CIE was caused by an overturn of a previously well-stratified ocean, releasing light dissolved inorganic carbon into the upper water column. Meyer et al. (2011) invoked that increased productivity in the water column generated a steeper surface to deep isotopic gradient, thus leading to more positive $\delta^{13}C_{carb}$-values.

The SSB is associated with widespread deposition of organic-rich sediments in China (Chen et al. 2011; Grasby et al. 2013a; Sun et al. 2015), Japan, Vietnam, Arctic Canada and Far East Russia (Galfetti et al. 2008; Shigeta et al. 2009; Komatsu et al. 2014). However, as noted by Sun et al. (2015), the temporal correlation between marine anoxia and the C-isotope record is still unresolved. Tethyan records from Iran suggested that peak anoxia developed just prior to the most negative C-isotope values (Horacek et al. 2007). SSB successions from Pakistan recorded anoxia in the uppermost Smithian when the C-isotope record shifted to positive values (Hermann et al. 2011; Romano et al. 2013). In Spitsbergen anoxic/euxinic conditions prevailed during the LSTM and during most of the early Spathian $\delta^{13}C$ maximum (Wignall et al. 2016). In records from South China, Meyer et al. (2011), in turn, showed anoxia peaking later when the C-isotopes reached their maximum values. Sun et al. (2015), on the other hand, recorded anoxia from the late Smithian to the early Spathian in South China, succeeded by a sharp transition to well-oxygenated conditions. They suggested that this shift was triggered by climatic cooling and oxygen increase driven by organic carbon and pyrite burial (Sun et al. 2015). Based on the co-variation between an ∼10–15 ‰ negative shift in $\delta^{34}S$ in

carbonate-associated sulfate and an ∼4 ‰ positive shift in $\delta^{13}C_{carb}$ in South China, Zhang et al. (2015) hypothesized that cooling-driven reinvigoration of oceanic overturning circulation led to stronger up-welling causing mixing of sulfide- and nutrient-rich deep waters into the upper ocean layer at the SSB, thus promoting both enhanced marine productivity and oxidation of advected H_2S. They estimated the duration of the Smithian–Spathian cooling event to ∼75–150 kyrs.

Information on changes in the terrestrial vegetation across the SSB have primarily been obtained from palynological records in marine successions in Norway (Galfetti et al. 2007b; Hochuli & Vigran, 2010), Tibet (Schneebeli-Hermann et al. 2012) and Pakistan (Hermann et al. 2012b), and these all show a shift from spore-dominated Smithian assemblages to palynofloras dominated by bisaccate pollen in the Spathian. In addition, biomarker data from South China (Saito et al. 2013) also indicate a shift to woody gymnospermous plants around the SSB. In the record from Pakistan, Hermann et al. (2012b) only recorded a temporary dominance of gymnosperm vegetation during late Smithian to earliest Spathian times, followed by a return to spore dominance (albeit lower than during the middle Smithian) during Spathian time. Both Hochuli & Vigran (2010) and Romano et al. (2013) interpreted the recorded shift from spore-dominating to pollen-dominating floras in late Smithian time as a shift from humid to dry conditions around the SSB.

Here we present new sedimentological, organic C-isotope and palynological records across the SSB from several marine outcrop sections and a drill core from the Wandel Sea Basin (WSB) in North Greenland. The herein investigated successions are constrained by palynology, ammonoid biostratigraphy and $\delta^{13}C_{org}$ chemostratigraphy, and provide an insight into the environmental conditions during Smithian to earliest Anisian times in the northern mid-latitudes.

2. Study area

During Early Triassic time the WSB was located around 45° N, on the northern margin of Pangaea, with the Sverdrup Basin to the west and the palaeo-Barents Sea area and Svalbard to the east and north (Bjerager et al. in press). The WSB formed the northern continuation of the Danmarkshavn Basin offshore Northeast Greenland, and the western continuation of basins in the southern part of the Barents Sea (Bjerager et al. in press). The exposed Triassic succession in the WSB spans a near complete Induan–Norian succession, which is up to 700 m in thickness (Bjerager et al. in press). The Triassic rests unconformably on Upper Permian carbonates and siliciclastic rocks of the Midnatfjeld Formation (Fig. 1) (Håkansson, 1979), and is erosionally overlain by Upper Jurassic – Lower Cretaceous siliciclastic rocks of the Ladegårdsåen Group. Smithian to lower Anisian strata are well exposed in Peary Land, with sections that crop out at Dunken, Hjulspordalen and also Henry Parish Bjerg. In addition, the interval is encompassed in the fully cored Dunken-2 borehole (Fig. 1). This paper focuses on the Hjulspordalen and Dunken-2 successions.

3. Methods

3.a. Total organic carbon and organic C-isotopes

The total organic carbon (TOC) of the samples was measured in two ways. TOC was determined by combustion using a LECO
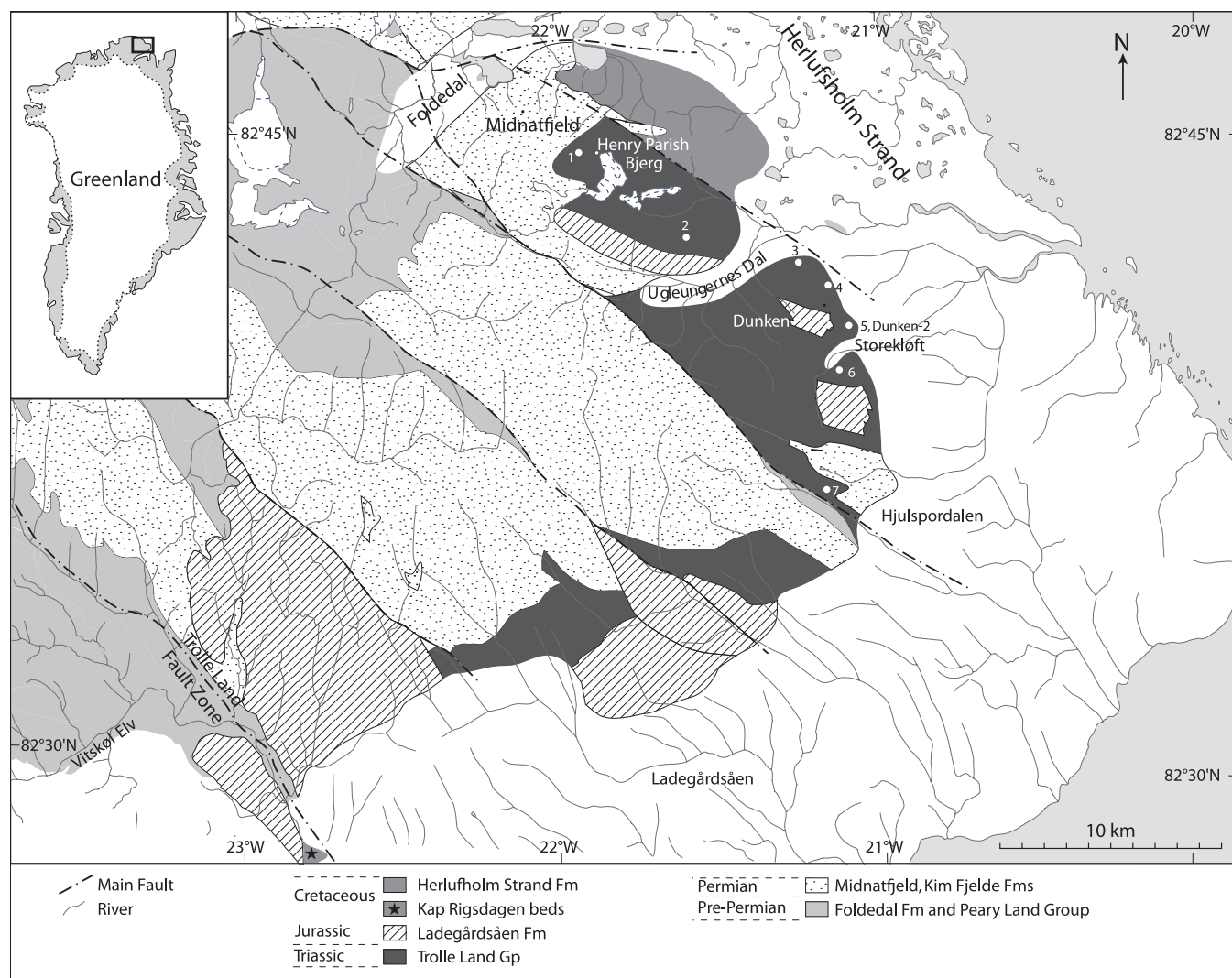
GN01_02_054_06_SLI_KimFjelde

Fig. 1. Map of North Greenland, Peary Land and localities mentioned in the text: (1) Henry Parish W; (2) Henry Parish Bjerg S; (3) Dunken Main; (4) Dunken-X; (5) Dunken-2 core; (6) Storekløft; (7) Hjulspordalen.

CS-200 induction furnace after elimination of carbonate-bonded carbon by prolonged HCl-treatment at 65 °C in two stages, followed by rinsing and drying at 90 °C. Initial aliquot size was 300 mg, and samples were ground to <250 micron prior to analysis. TOC was also determined as an integral part of stable carbon isotopic analysis, where an estimation of the TOC was also carried out prior to the organic C-isotope analysis. The samples were then ground where necessary to a fine powder and then acidified with 1M hydrochloric acid and left overnight to allow inorganic carbon to be liberated as CO_2. The samples were then neutralized by repetitively washing with distilled water and subsequently oven dried at 60 °C prior to $\delta^{13}C$ isotope analysis. The total ion beam data from the organic C-isotope analysis was used to determine the carbon content of the acid-washed samples. This data along with the weight loss data from the acid washing was used to calculate the organic carbon content (TOC) for each sample. The results of the two methods are in accordance in the Dunken-2 section, albeit with the LECO CS-200 method displaying somewhat lower values throughout (Fig. 2). However, for the Hjulspordalen section the results of the two methods vary

significantly within a part of the section, with the LECO CS-200 method displaying generally higher TOC values (Fig. 3).

The C-isotope analyses were performed using an elemental analyser – isotope ratio mass spectrometer (EA-IRMS; Europa Scientific 20-20 IRMS) at ISO-Analytical Limited, UK. The reference material used was IA-R001 (wheat flour, $\delta^{13}C_{V\text{-}PDB} = -26.43$ ‰). For quality control purposes check samples of IA-R001, IA-R005 (beet sugar, $\delta^{13}C_{V\text{-}PDB} = -26.03$ ‰) and IA-R006 (cane sugar, $\delta^{13}C_{V\text{-}PDB} = -11.64$ ‰) were analysed during batch analysis of the samples. IA-R001, IA-R005 and IA-R006 are calibrated against and traceable to IAEA-CH-6 (sucrose, $\delta^{13}C_{V\text{-}PDB} = -10.43$ ‰). IAEA-CH-6 is an inter-laboratory comparison standard distributed by the International Atomic Energy Agency (IAEA), Vienna. Tin capsules containing sample or reference material were loaded into an auto-sampler and dropped in sequence into a furnace held at 1000 °C and combusted in an oxygen-rich environment, raising the temperature in the region of the sample to ~1700 °C. The gases produced on combustion were swept in a helium stream over a combustion catalyst (Cr_2O_3), with copper oxide wires to oxidize hydrocarbons and
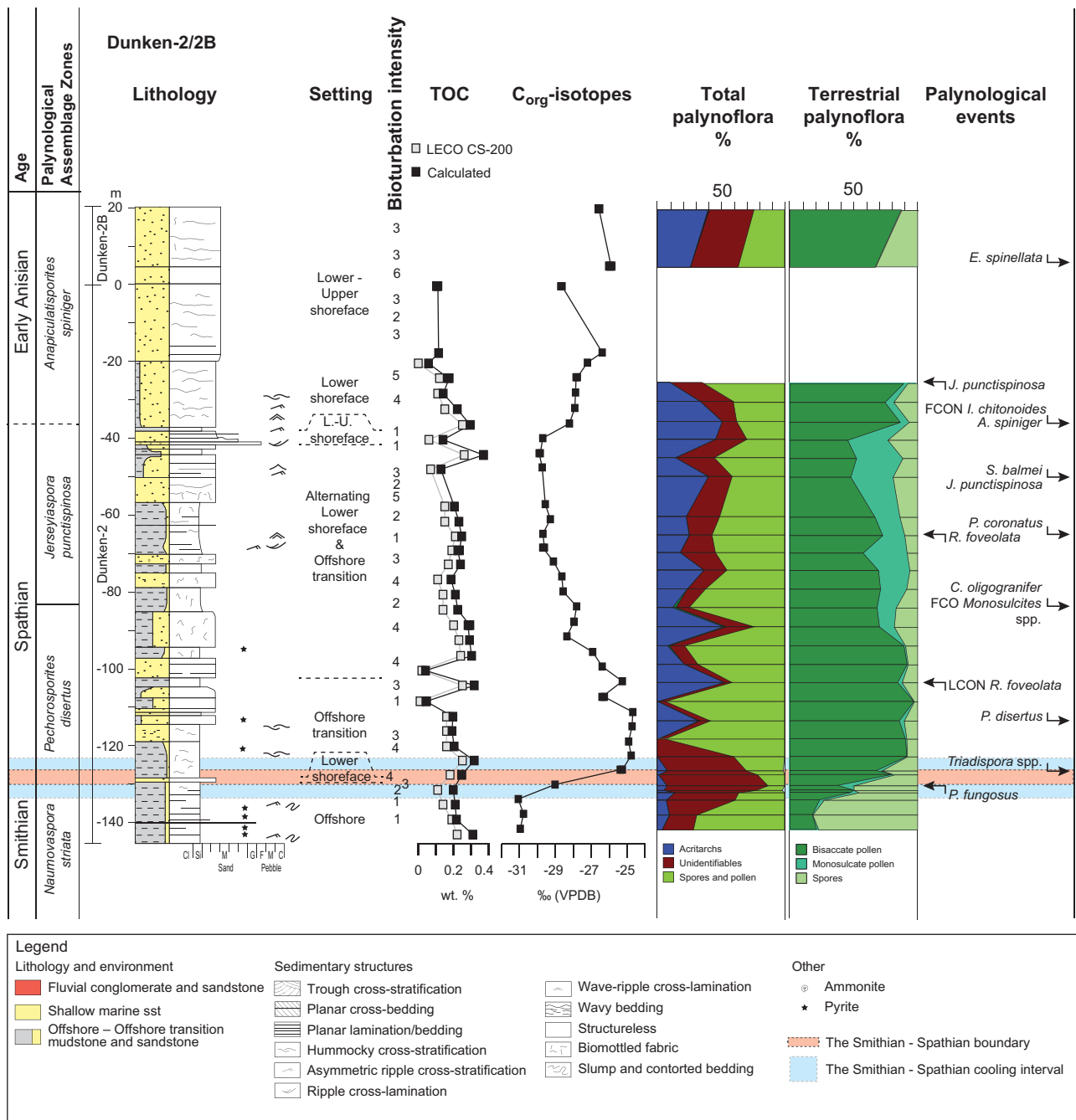
Fig. 2. Lithology, depositional setting, chemo- (δ¹³C_org) and biostratigraphy (palynology), as well as palynofloral changes, of the Smithian–lower Anisian succession of the Dunken-2 core.

silver wool to remove sulfur and halides. The resultant gases, N_2, NO_x, H_2O, O_2 and CO_2, were swept through a reduction stage of pure copper wires held at 600 °C. This step removed O_2 and converted NO_x species to N_2. A magnesium perchlorate chemical trap removed water. Carbon dioxide was separated from nitrogen by a packed column gas chromatograph held at an isothermal temperature of 100 °C. The resultant CO_2 chromatographic peak entered the ion source of the EA-IRMS where it was ionized and accelerated. Gas species of different mass were separated in a magnetic field then simultaneously measured using a Faraday cup collector array to measure the isotopomers of CO_2 at m/z 44, 45 and 46. Both references and samples were converted and analysed in this

manner. The analysis proceeded in a batch process, whereby a reference is analysed followed by a number of samples and then another reference.

3.b. Palynology

The samples were prepared at the Geological Survey of Denmark and Greenland using standard palynological methods involving digestion of 20 g of sediment in hydrochloric and hydrofluoric acid, mild oxidation and filtering of the organic residues through a 11 μm mesh filter. Two to three strew slides were mounted per sample, using glycerine gel as a mounting medium. The
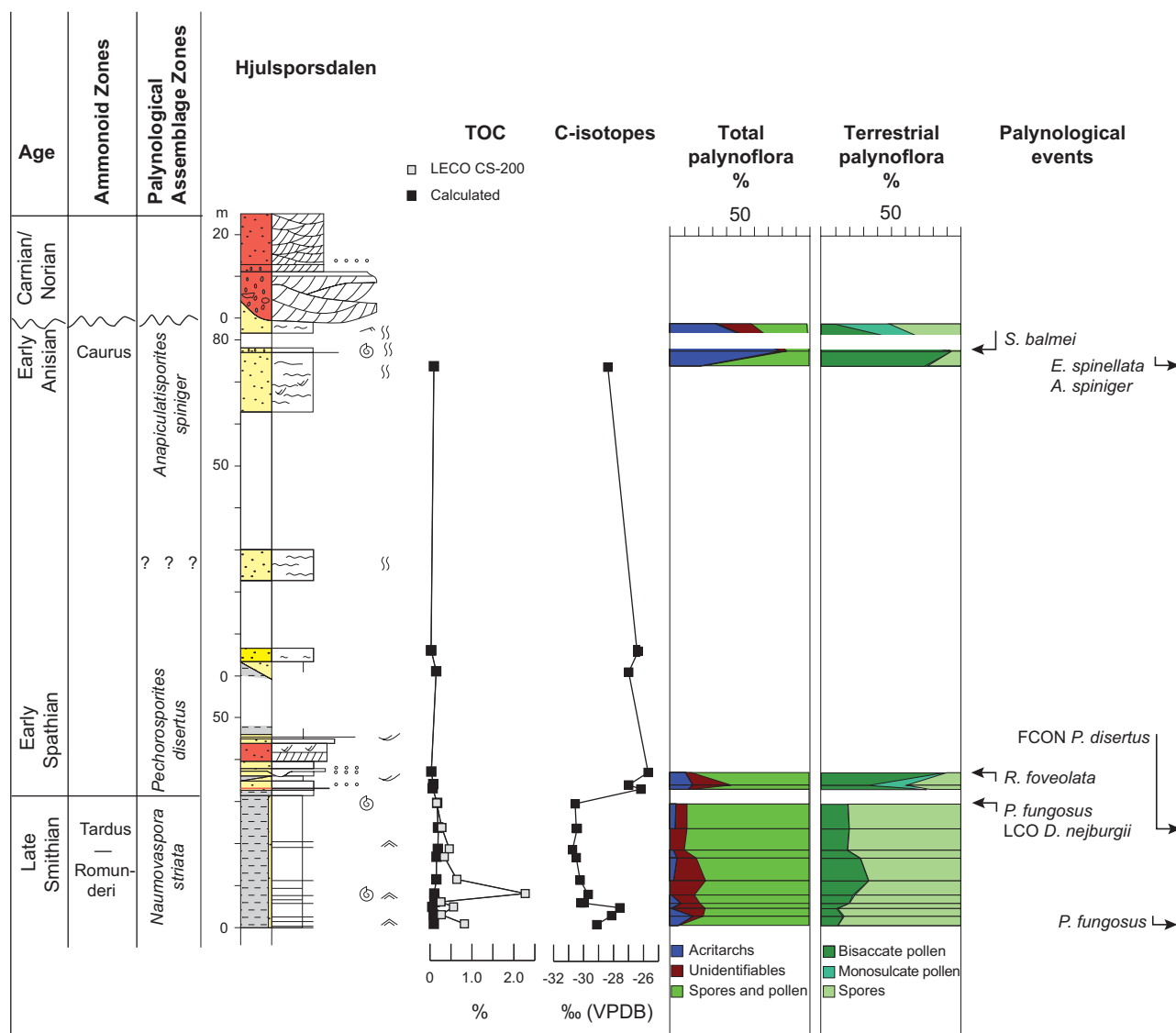
Fig. 3. Litho-, chemo- ($\delta^{13}C_{org}$) and biostratigraphy (palynology and ammonoids), as well as palynofloral changes, of the Smithian–lower Anisian succession at Hjulspordalen. Legend can be found in Figure 2.

quantitative palynological analysis was carried out on one or more strew slides from each sample using a Leica DM 2000 transmitted light microscope fitted with a differential interference contrast system. During counting, the strew slides were scanned systematically using a ×40 lens (506097, Leica) along transverse transects, until the entire slide was scanned or until 300 specimens or more were counted. Higher magnification was used when necessary for identification of specific taxa. The remaining strew slides from each sample were systematically scanned in order to register taxa not encountered during the counting. For analysis of the palynofloral changes, the spores and pollen were grouped in three major groups: spores, non-saccate pollen and bisaccate pollen.

4. Results

4.a. Stratigraphic framework

Strata exposed at the Dunken and Hjulspordalen outcrop sections (Figs 2, 3) are constrained by the presence of ammonoids, including *Arctoceras blomstrandi* (Fig. 4), to the middle to late Smithian

Romunderi–Tardus zones (Tozer, 1994). The Dunken section samples were found to be palynologically barren, but the Smithian strata at Hjulspordalen contain a diverse and fairly well-preserved palynoflora dominated by spores, mainly *Densoisporites* spp., *Lundbladispora* spp. and the very characteristic *Punctatisporites fungosus* (Fig. 5), enabling correlation with the *Naumovaspora striata* Composite Assemblage Zone of Vigran *et al.* (2014). The palynoflora from the lowermost part of the Dunken-2 core is very poorly preserved; however, the presence of abundant *Punctatisporites fungosus* indicates a Smithian age. The last occurrence of *Punctatisporites fungosus* occurs at 129.92 m in the Dunken-2 core, and at 29.50 m in the Hjulspordalen section, and serves as a good marker for the top of the Smithian in Peary Land (Figs 2, 3). It should be noted that *P. fungosus* was sporadically registered in Spathian and Anisian strata by Vigran *et al.* (2014), but was only found to be abundant in the *Naumovaspora striata* Composite Assemblage Zone.

The SSB is placed at the top of the *Naumovaspora striata* Composite Assemblage Zone of Vigran *et al.* (2014), which is
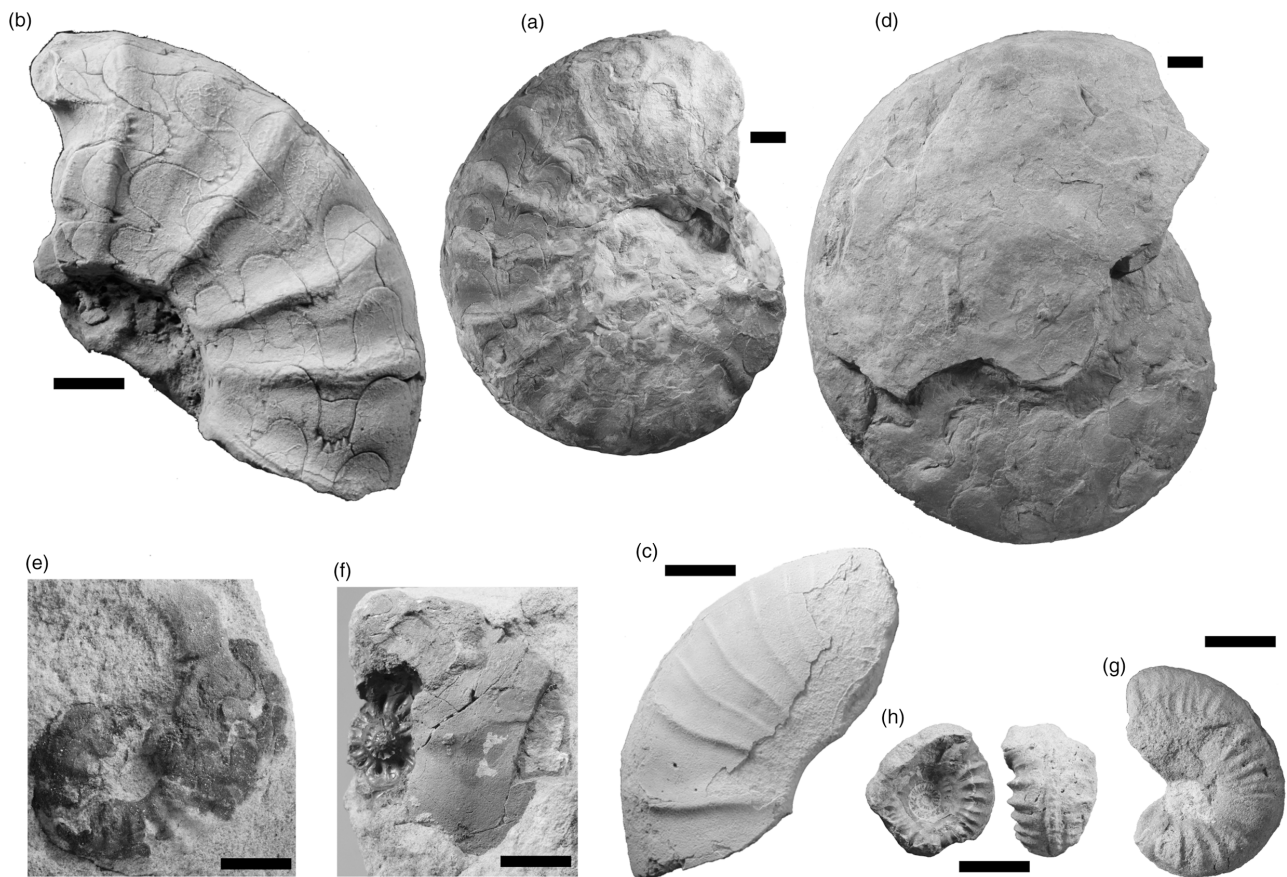
Fig. 4. Ammonoids from the Smithian–lower Anisian of Peary Land. (a–c) *Arctoceras blomstrandi* (Lindstroem), MGUH 33328–30 all from GEUS 539291b. (d) *Radioceras?*, MGUH 33331 from GEUS 543701. (e) *Lenotropites caurus* (McLearn), MGUH 33332 from 542733. (f) *Lenotropites tardus* McLearn, MGUH 33333 from GEUS 542740. (g) *Groenlandites* cf. *nielseni* Kummel, MGUH 33334 from GEUS 519202. (h) *Pearylandites* aff. *troelseni* Kummel, MGUH 33335 from GEUS 519202.

located between 129.92 and 127.07 m in the Dunken-2 core. However, at Hjulspordalen the topmost part of the Smithian and lowermost part of the Spathian is probably missing (Fig. 3). Palynological assemblages assigned to the early Spathian *Pechorosporites disertus* Composite Assemblage Zone of Vigran *et al.* (2014) were identified in Hjulspordalen and in the Dunken-2 core. The palynofloras from Hjulspordalen are fairly well preserved, while those from Dunken-2 are poorly preserved. In Dunken-2, high abundances of unidentifiable palynomorphs also characterize the palynoflora in the lowermost Spathian, but decrease upsection. The terrestrial palynoflora differs from the underlying Smithian one, in being dominated by bisaccate pollen instead of spores. Taeniate bisaccate pollen, mainly *Lunatisporites* spp. and *Protohaploxypinus samoilovichii*, are abundant (Fig. 5). The characteristic spore *Rewanispora foveolata* is also common within this interval (Fig. 5). In the Dunken-2 core the *Pechorosporites disertus* Composite Assemblage Zone can be recognized up to 83.61 m where *Cyclotriletes oligogranifer* is registered for the first time, indicating assignment to the late Spathian *Jerseyiaspora punctispinosa* Composite Assemblage Zone of Vigran *et al.* (2014), although the nominate taxon is first registered at 49.53 m (Fig. 2). The first occurrences of *Anapiculatisporites spiniger* and *Illinites chitonoides* occur at 35.23 m in the Dunken-2 core, marking the lower boundary of the *Anapiculatisporites spiniger* Composite Assemblage Zone of Vigran *et al.* (2014).

Palynofloras indicative of the early Anisian *Anapiculatisporites spiniger* Composite Assemblage Zone have also been recognized in the Dunken-2B outcrop section, in the lowermost part of the Dunken-X outcrop section, in the lowermost part of the Storekløft-3 succession, at Henry Parish Bjerg W, Henry Parish Bjerg S and in two samples from Hjulspordalen (Fig. 3). At Storekløft-3 and Hjulspordalen this age assignment is further confirmed by the presence of ammonoids assigned to the early Anisian Caurus Zone of Tozer (1994) (Fig. 4).

4.b. Sedimentology and depositional evolution

The Smithian–lower Anisian sedimentary succession in Peary Land forms an overall shallowing-upward succession from offshore mudstones in the Smithian to upper shoreface sandstones in the lower Anisian, with several internal transgressive–regressive trends recorded in the Dunken-2 core (Fig. 2). Bioturbation intensity in the core was assessed using the semi-quantitative six-point ichnofabric index (II) scheme of Droser & Bottjer (1986) and this is shown on Figure 2.

4.b.1. Smithian

The Smithian mudstones are dark grey and laminated and contain frequent soft-sediment deformations, e.g. slump structures and contorted bedding (Fig. 6a). They are commonly without trace fossils (bioturbation intensity 1; Fig. 6a); but occasionally *Planolites*, *Chondrites* and spreite structures that may represent *Zoophycos* occur (Fig. 6b). Sand laminae and sand lenses with sharp boundaries increase in frequency upsection. Pyrite is also present. An
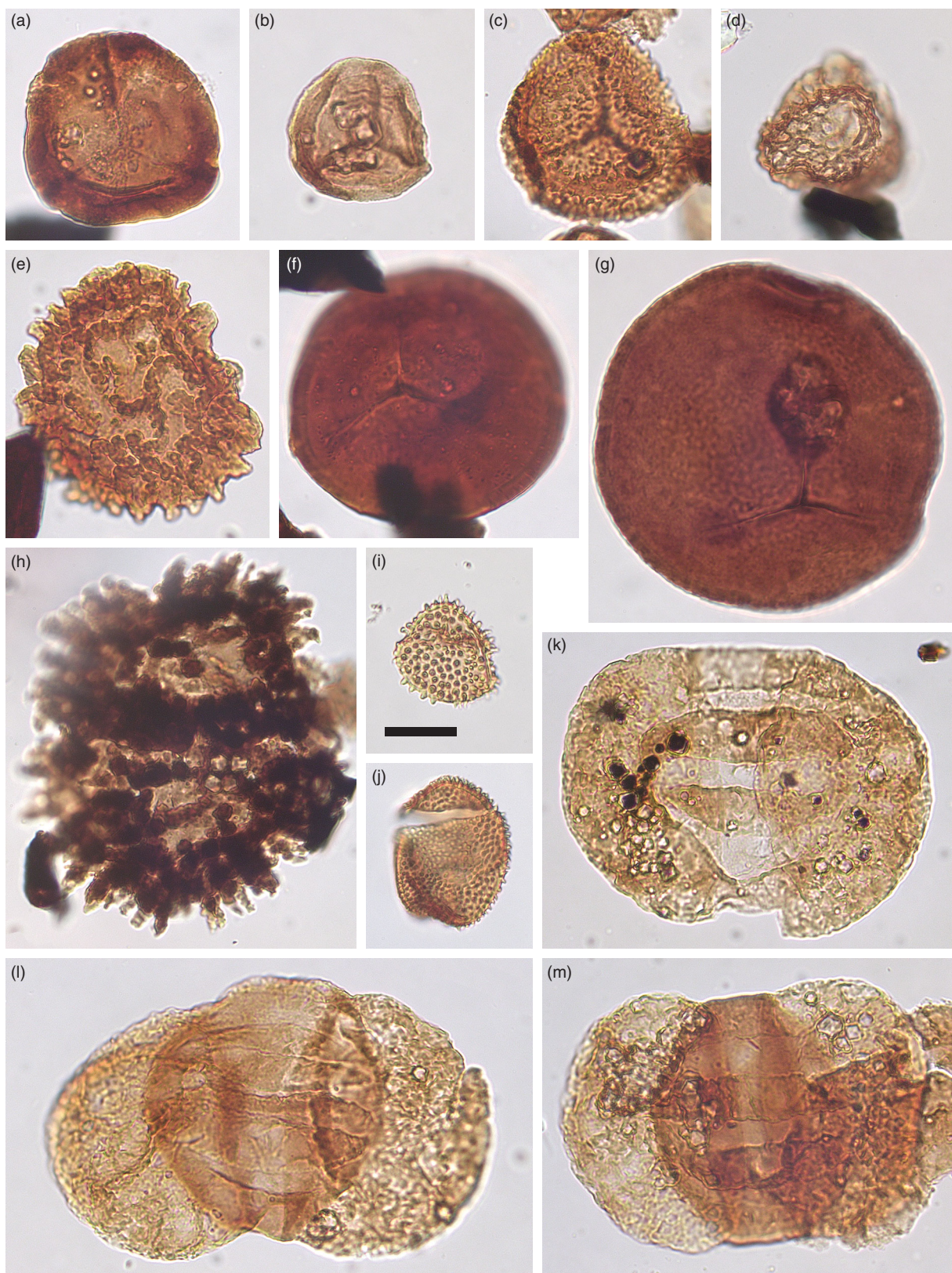
Fig. 5. Selected spores and pollen from (a–g, i–m) Hjulspordalen and (h) Dunken-2. Taxa names are followed by sample and slide number and England Finder coordinates. (a) *Densoisporites playfordii*, 537288:5, M52/3; (b) *Densoisporites nejburgii*, 537280:5, E44/3; (c) *Lundbladispora willmottii*, 537288:5, V53/1; (d) *Rewanispora foveolata*, 519201:4, J56/4; (e) *Pechorosporites disertus*, 537288:5, M50/4; (f) *Punctatisporites fungosus*, 537288:5, Z45/2; (g) *Punctatisporites fungosus*, 537280:5, F43/3; (h) *Jerseyiaspora punctispinosa*, dyad, Dunken-2 44.65 m, L43/2; (i) *Anapiculatisporites spiniger*, 537296:3, G27/3; (j) *Eresinia spinellata*, 537296:3, G44/3; (k) *Lunatisporites pellucidus*, 537288:5, V35/2; (l) *Protohaploxypinus samoilovichii*, 537288:5, U42/2; (m) *Lunatisporites noviaulensis*, 537288:5, F19/4. Scale bar in (i) is 20 μm and applies to all photographs.
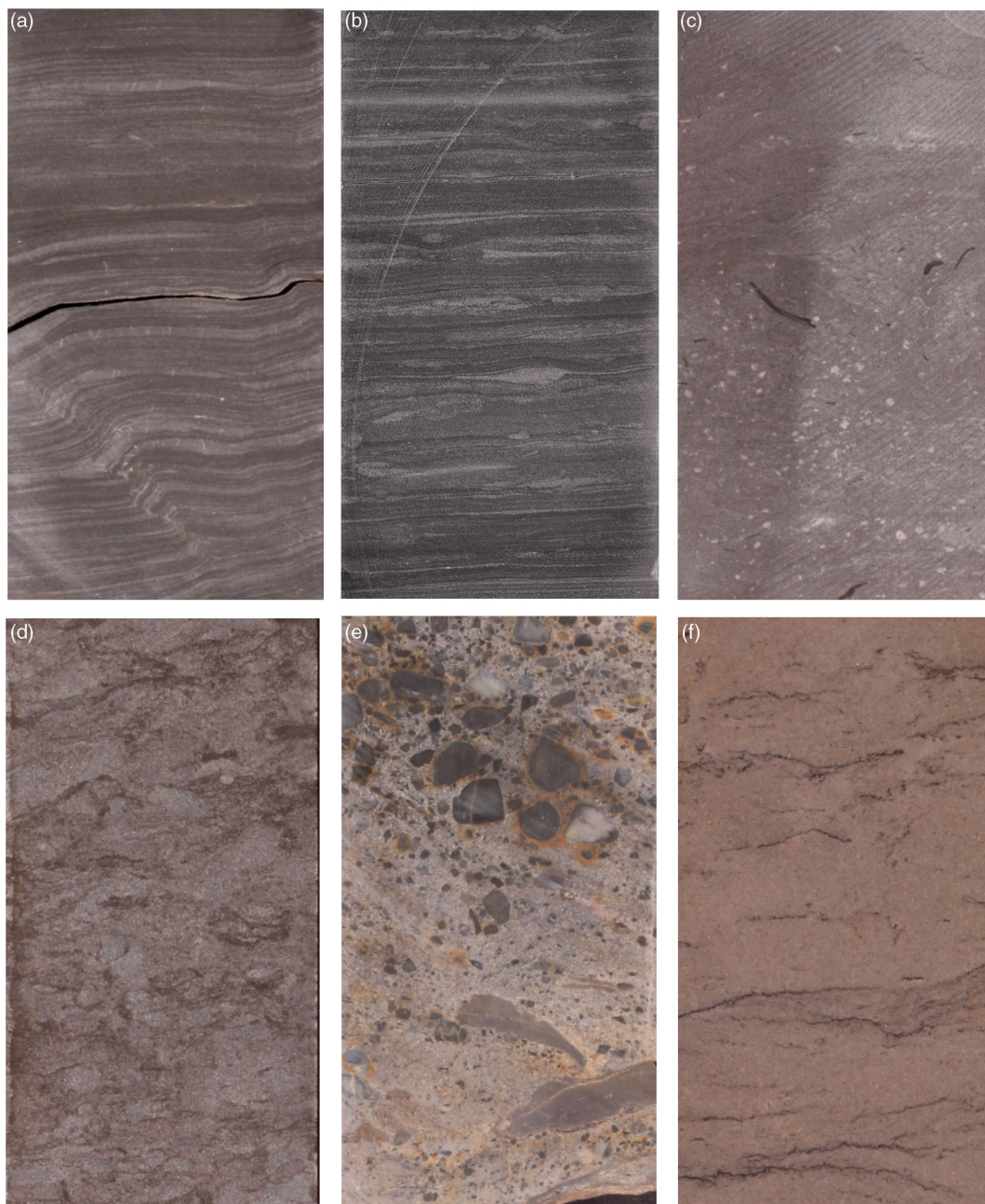
Fig. 6. Dunken-2 core photos, core width *c.* 42 mm: (a) laminated mudstone with sand laminae, deformed bedding in the lower part (depth 140.2 m); (b) laminated mudstone with thin sandstone laminae and minor amounts of trace fossils of *Chondrites* and compressed *Planolites* (depth 132.3 m); (c) biomottled sandy mudstone with dispersed black and white bioclasts (depth 119.3 m); (d) intensely biomottled heterolith, sandstone dominated (depth 89.55 m); (e) pebbly sandstone overlain by pebble conglomerate, clasts comprise mainly quartzite and chert (depth 40.54 m); (f) homogeneous sandstone with common stylolites (depth 19.45 m).

erosional pebble lag, a few centimetres thick, is present in the lowermost part of the core. The mudstones are interpreted as offshore deposits on a gently sloping seafloor with frequent deposition of thin storm sand laminae or distal turbidites. The pebble lag probably represents an erosional transgressive lag, and the succeeding fine planar laminated mudstones represent a maximum flooding zone in the Smithian.

4.b.2. The Smithian–Spathian boundary (SSB) interval
Just below the palynologically defined SSB interval, the bioturbation index increases from 1 to 3 in the core. A 1.2 m thick erosional and intensely biomottled sandstone bed (bioturbation index 4), with a thin coarse-grained lag at the base, occurs at 128.9 m. The biomottled sandstone contains common *Planolites* and *Rhizocorallium* and is interpreted as a regressive unit in a lower shoreface setting with a sequence boundary at the base. The equivalent interval in the Hjulspordalen section comprises shallow-marine sandstones. The biomottled sandstone is overlain by dark grey to grey, moderately bioturbated, sandy mudstone (Fig. 6c), with thin fine-grained sandstone beds and lamina. Trace fossils include *Chondrites* and *Rhizocorallium*, characteristic of the *Cruziana* ichnofacies, which together with the sedimentology indicate an offshore transition zone with a frequent influx of tempestites.

4.b.3. Lower to middle Spathian

The Dunken-2 core records a nearly 100 m thick Spathian interval of alternating units of massive to faintly bedded sandstones, biomottled sandstones, heteroliths and mudstones that were deposited in environments fluctuating between offshore transition and lower shoreface (Figs 2, 6d). Massive to faintly bedded fine-grained sandstones occur as distinct beds, 10 cm to about 1 m thick, interbedded with mudstones. The sandstones commonly show planar bedding, wavy bedding or ripple lamination in the top part, occasionally with a weakly to moderately biomottled top draped by mudstone. The facies occur in the intervals 108–97 m and 53–41 m, and are interpreted as mainly high-density gravity flows, with occasional low-density flows in the top part.

Biomottled sandstones, muddy sandstones and sandstone-dominated heteroliths compose the main sandstone-dominated facies types in the interval and are interbedded with mudstones. Beds vary between a few centimetres and up to 3 m in thickness, with occasionally wavy bedding and ripple lamination visible, and individual beds are commonly draped by mudstones. Water escape structures and slumping are rarely observed. The degree of biomottling varies mainly between moderate and intense, and diagnostic trace fossils include *Thalassinoides*, *Planolites*, *Chondrites*, *Rhizocorallium* and *Scolicia*. The sandstone distribution is dominant in the intervals 114–105 m, 102–97 m, 94–85 m, 79–71 m and 57–41 m. The sandstones are interpreted as having been deposited by gravity flows and storm beds in a lower shoreface to offshore transition setting with an intense burrowing activity in oxic seafloor conditions. The bioturbation intensity peaks around 55 m and 20 m (bioturbation intensity 5) (Fig. 2).

Mudstone-dominated heteroliths and mudstones compose units of centimetres to several metres in scale. The muddy sediments are generally moderate to intensely biomottled with visible trace fossils dominated by *Chondrites* and common to abundant *Rhizocorallium*, *Thalassinoides* and *Planolites*. Abundant thin sandstone beds, laminae and streaks are present showing faint plane bedding, wavy bedding and occasionally ripple lamination. This facies is mainly distributed in the intervals 105–102 m, 97–94 m, 85–79 m and 70–57 m, and is interpreted as having been deposited from suspension in an oxygenated offshore transition environment allowing a diverse and intense biomottling. The thin sandstone beds are interpreted as having been deposited during storms and as low-density gravity flows. An erosive pebble conglomerate, 2 cm thick, occurs at 94 m. It is clast supported with rounded clasts and a muddy sand matrix and common pyrite. It is interpreted as an erosional transgressive lag. Mudstones, plane and wavy bedded, with thin sandstone laminae compose minor parts of the interval. The facies may have a weak biomottled fabric of *Chondrites*, *Planolites* and *Thalassinoides*. The facies occur predominantly in the intervals 70–62 m, 50–49 m and 45–42 m. The mudstones are interpreted as having been deposited from suspension in a distal offshore transition environment.

4.b.4. Upper Spathian

A prominent pebble conglomerate, 20 cm thick, with common clasts of chert, mudstones and sandstones occurs at 40.54 m (Fig. 6e). It is overlain by a 3.3 m thick fining upwards interval of coarse-grained to fine-grained sandstones with planar, wavy and low-angle ripple laminations and common mud drapes, and a mudstone-dominated heterolith, with faint planar and wavy bedding in the top. The lower part of the interval from 41–37 m is interpreted as having been deposited in a shallow-marine wave- and current-influenced environment. The mudstone-dominated heteroliths are interpreted as having been deposited in an offshore transition environment.

4.b.5. Lower Anisian

The lower part of the Anisian is recorded in the Dunken-2 core, and in the outcrop section Dunken-2B adjacent and stratigraphically above the cored interval (Fig. 2). A regressive pebbly lag deposit marks the base of the overlying interval, 37–20 m, which consists of sandstone-dominated heteroliths. The interval shows wavy and indistinct bedding in the lower parts and an increasing degree of biomottling upwards. It is topped by a homogeneous bed, 20 cm thick, which in turn is overlain by a burrowed horizon about 40 cm thick. The biomottled sandstone-dominated heterolith is interpreted as having been deposited in a lower shoreface environment. The overlying succession is represented by quartz-dominated sandstones with common stylolites, and only minor biomottling (Fig. 6f). Occasionally, planar bedding or low-angle cross-bedding are observed. Thin muddy beds are recorded in the upper part of the core. This interval is interpreted as having been deposited in lower–upper shoreface environments.

4.c. TOC and $\delta^{13}C_{org}$

The TOC and organic C-isotope data analysed herein are shown in Table 1. The TOC values of the Dunken-2 core are generally low, <0.4 %, as indicated by both TOC techniques (Figs 2, 3). In Hjulspordalen there is some divergence between TOC values determined by the different methods. Generally TOC values are below 1 wt %, but the LECO CS-200 data are generally higher within the Smithian part of the succession (up to 2.27 wt %). TOC determined as part of stable isotopic analysis yielded very low values compared to values yielded by dedicated TOC analysis, which shows higher and more scattered values. The difference may possibly be attributed to sample size and representativity. Samples with low and unevenly distributed contents of organic carbon are commonly susceptible to representativity problems when the aliquot size is very small. Except for the section mentioned, TOC data from the two different methods agree very well.

The Smithian C-isotope records exhibit relatively consistent negative values between −29.69 ‰ and −30.49 ‰ (Figs 2, 3). The Dunken Main succession exhibits similar negative organic C-isotope values, reaching a minimum value of −31.16 ‰. In addition, similar negative organic C-isotope values were retrieved from the lowermost part of the Dunken-2 core, with values varying between −31.06 ‰ and 29.02 ‰ marking the top of the Smithian negative excursion. This is succeeded by an interval with consistently more positive values, −25.40 ‰ to −24.70 ‰ in the lower Spathian, followed by increasingly more negative values, culminating at −29.90 ‰ in the upper Spathian. In the Hjulspordalen record, C-isotope values around −26 ‰ within the *Pechorosporites disertus* Zone are correlated with the onset of the middle–upper Spathian negative trend in the Dunken-2 record (Figs 2, 3). In the lowermost Anisian the organic C-isotope curve exhibits a return to less depleted values, up to −26.40 ‰. A sample from the top of the Dunken-2 core shows a value of −28.66 ‰ (Fig. 2). Similarly, a value of −28.38 ‰ is registered in the early Anisian Caurus ammonite Zone at Hjulspordalen (Fig. 3).

4.d. Palynofloral changes

The marine versus terrestrial palynology shows similar trends in the two records from North Greenland. Marine phytoplankton, primarily *Michrystridium* and *Lophosphaeridium*, normally

Table 1. TOC and organic C-isotope values of the samples from the Hjulspordalen and Dunken-2/2B successions

Sample No.	Height/depth in metres	Locality	δ¹³C ‰ ᵥ₋ₚ𝒹ᵦ	Organic carbon content (TOC) in wt %	TOC (LECO CS200) in wt %
537296	134.00	Hjulspordalen 2	−28.38	0.093	-
537295	66.00	Hjulspordalen 1	−26.43	0.026	-
537295	66.00	Hjulspordalen 1	−26.35	0.029	-
537294	61.00	Hjulspordalen 1	−26.99	0.148	-
537293	37.00	Hjulspordalen 1	−25.69	0.032	-
537292	34.00	Hjulspordalen 1	−26.99	0.078	-
519201	33.00	Hjulspordalen 2	−26.18	0.063	-
537290	29.50	Hjulspordalen 2	−30.56	0.171	0.16
537289	23.60	Hjulspordalen 2	−30.49	0.191	0.28
537289	23.60	Hjulspordalen 2	−30.42	0.199	0.28
537288	18.50	Hjulspordalen 2	−30.74	0.188	0.46
537287	16.60	Hjulspordalen 2	−30.49	0.155	0.34
537286	11.20	Hjulspordalen 2	−30.23	0.151	0.64
537285	7.80	Hjulspordalen 2	−29.69	0.103	2.27
537284	5.80	Hjulspordalen 2	−29.98	0.108	0.26
537284	5.80	Hjulspordalen 2	−30.18	0.105	0.26
537283	4.60	Hjulspordalen 2	−27.58	0.055	0.56
537281	2.73	Hjulspordalen 2	−28.13	0.088	0.27
537280	0.55	Hjulspordalen 2	−29.12	0.091	0.82
542745	20.00	Dunken-2B	−26.57	0.082	-
542742	5.00	Dunken-2B	−25.90	0.096	-
542742	5.00	Dunken-2B	−25.99	0.105	-
517006-239	−0.41	Dunken-2	−28.70	0.103	-
517006-239	−0.41	Dunken-2	−28.63	0.111	-
517006-240	−17.63	Dunken-2	−26.40	0.115	-
517006-051	−20.26	Dunken-2	−27.22	0.058	0.00
517006-055	−24.06	Dunken-2	−27.78	0.170	0.12
517006-055	−24.06	Dunken-2	−27.85	0.175	-
517006-059	−28.02	Dunken-2	−27.88	0.141	0.11
517006-063	−32.05	Dunken-2	−27.92	0.221	0.15
517006-067	−36.08	Dunken-2	−28.22	0.294	0.25
517006-071	−39.89	Dunken-2	−29.70	0.140	0.06
517006-075	−43.81	Dunken-2	−29.84	0.369	0.26
517006-075	−43.81	Dunken-2	−29.90	0.369	-
517006-079	−47.49	Dunken-2	−29.73	0.128	0.07
517006-083	−57.04	Dunken-2	−29.56	0.204	0.15
517006-087	−60.95	Dunken-2	−29.28	0.230	0.15
517006-091	−64.75	Dunken-2	−29.69	0.246	0.21
517006-095	−68.33	Dunken-2	−29.61	0.233	0.19
517006-095	−68.33	Dunken-2	−29.70	0.224	-
517006-099	−71.94	Dunken-2	−29.11	0.239	0.17
517006-103	−75.82	Dunken-2	−28.64	0.185	0.11
517006-107	−79.71	Dunken-2	−28.57	0.210	0.14

(*Continued*)

Table 1. (*Continued*)

Sample No.	Height/depth in metres	Locality	δ¹³C ‰ V-PDB	Organic carbon content (TOC) in wt %	TOC (LECO CS200) in wt %
517006-111	−83.61	Dunken-2	−27.82	0.223	0.14
517006-115	−87.59	Dunken-2	−27.96	0.292	0.20
517006-115	−87.59	Dunken-2	−27.97	0.282	-
517006-119	−91.41	Dunken-2	−28.36	0.290	0.23
517006-123	−95.45	Dunken-2	−26.93	0.302	0.24
517006-127	−99.24	Dunken-2	−26.40	0.041	0.02
517006-131	−103.07	Dunken-2	−25.28	0.317	0.25
517006-135	−107.13	Dunken-2	−26.41	0.047	0.01
517006-135	−107.13	Dunken-2	−26.28	0.043	-
517006-139	−111.08	Dunken-2	−24.70	0.196	0.16
517006-143	−114.78	Dunken-2	−24.74	0.191	0.16
517006-147	−118.74	Dunken-2	−24.93	0.203	0.16
517006-151	−122.37	Dunken-2	−24.79	0.317	0.25
517006-155	−126.04	Dunken-2	−25.28	0.245	0.18
517006-155	−126.04	Dunken-2	−25.40	0.246	-
517006-159	−129.92	Dunken-2	−29.02	0.198	0.11
517006-163	−133.68	Dunken-2	−31.06	0.209	0.14
517006-167	−137.53	Dunken-2	−30.77	0.216	0.19
517006-171	−141.40	Dunken-2	−30.95	0.309	0.22

compose less than 10 % of the total palynoflora in the Smithian. From the lower Spathian and upsection the relative abundance of marine phytoplankton shows a general increasing trend, but with strong fluctuations. In the upper Spathian marine phytoplankton constitute up to 50 % of the total assemblage. The generally lower abundances of marine phytoplankton in the Hjulspordalen succession indicate a more proximal position for this locality. The relative abundance of unidentifiable palynomorphs is high around the SSB, reaching a maximum abundance of >85 % in the uppermost Smithian of the Dunken-2 core.

The late Smithian terrestrial palynoflora is totally dominated by spores in both records: up to 80 % in the Dunken-2 core and around 90 % at Hjulspordalen. Cavate lycophyte spores, primarily *Densoisporites nejburgii* and *Lundbladispora* spp. are dominant, and the fern spore *Punctatisporites fungosus* is abundant. Other fern spores include *Dictyophyllidites mortoni* and *Punctatisporites globosus*, but these are never abundant. In the Dunken-2 core, the palynoflora changes gradually across the SBB, with increased amounts of unidentifiable palynomorphs due to poor preservation in the uppermost Smithian. Contemporaneous to this change in organic matter preservation in the uppermost Smithian, there is also a gradual increase in the relative abundance of bisaccate pollen, which continues across the SSB. In the Dunken-2 record, a gradual increase in bisaccate pollen commenced in the uppermost Smithian, prior to the SSB (Fig. 2). The gradual increase in bisaccate pollen continued in the lowermost Spathian reaching abundances of ~90–95 % in the lower Spathian (Fig. 2). Bisaccates are represented by corystosperm pollen assigned to *Alisporites* spp. and *Falcisporites* spp., and conifer pollen *Lunatisporites pellucidus*, *L. noviaulensis* and *Protohaploxypinus samoilovichii*. From the middle Spathian to the upper Spathian there is a relative increase in non-saccate, primarily monosulcate pollen of ginkgoalean or cycadalean affinity in the Dunken-2 record, with a

subsequent relative decrease in bisaccate pollen, while the amount of spores remains relatively stable throughout the Spathian–lower Anisian. In the lowermost Anisian, non-saccate pollen decrease again abruptly and become virtually absent in the lower Anisian (Fig. 2). Although only sporadic spore-pollen assemblages are recorded from the lower Spathian and lower Anisian at Hjulspordalen, these appear to corroborate the changes recorded in the Dunken-2 core (Figs 2, 3).

5. Discussion

5.a. *Densoisporites nejburgii* and climate interpretations

In NW Europe and elsewhere, Smithian palynofloras are dominated by *Densoisporites nejburgii* (Kürschner & Herngreen, 2010), a spore known to have been produced by pleuromeiacean lycophytes (Balme, 1995). The palaeoecological preferences of the lycopsid *Pleuromeia*, described as a succulent quillwort by Grauvogel-Stamm (1999), is not entirely clear. Species of *Pleuromeia* are known to have produced two different types of spores: the trilete cavate spore *D. nejburgii* and monolete cavate spores assigned to *Aratrisporites* spp. (Balme, 1995). Anatomical features of the Pleuromeiaceae indicate that at least some species were halophytes (salinity tolerant) that inhabited coastal areas (Retallack, 1975). This seems to be supported by the fact that the Pleuromeiaceae also produced spores assigned to the form genus *Aratrisporites*, which are especially abundant in Lower Triassic shallow-marine strata (Balme, 1995). An abundance of *D. nejburgii* together with an acme of acritarchs in sediments deposited during the Smithian transgression in Germany, Poland and the Dolomites further seems to corroborate a coastal preference for the Pleuromeiaceae (Schulz, 1964; Visscher, 1974; Orlowska-Zwolińska, 1984; Fijałkowska, 1994; Fijałkowska-Mader, 1999;

Kürschner & Herngreen, 2010). Several authors have attributed *D. nejburgii* to xerophytic (dry-tolerant) floral elements, stating that *D. nejburgii* is more abundant in arid and semi-arid environments in especially low latitudes (Galfetti *et al.* 2007b; Hochuli & Vigran, 2010). In general, lycopsids are considered to be hygrophytic plants, but there are examples of lycopsids that are extremely desiccation tolerant, e.g. *Selaginella lepidophylla* of the Selaginellaceae, which can survive prolonged drought events retaining only <10 % of its water content (VanBuren *et al.* 2018). Hence, it is possible that the *Pleuromeia* that produced *D. nejburgii* spores was in fact xerophytic compared to many other lycopsids. Here, we use the relative abundance of *D. nejburgii* in palynofloras as an indicator of at least seasonally dry conditions, and complement this with other palaeoclimatic information from the Smithian to the Anisian (Table 2). The resulting interpretations for the LSTM, the Smithian–Spathian cooling and the early Spathian period, respectively, are plotted on palaeogeographic maps in Figure 8.

5.b. The Late Smithian Thermal Maximum

By comparing the Early Triassic $\delta^{18}O_{apatite}$-isotope record with temperature tolerance of animals and plants, Sun *et al.* (2012) came to the conclusion that equatorial temperatures during late Smithian time reached extreme values of up to 38 °C in the upper water column, with surface waters perhaps reaching 40 °C. The extreme heat in equatorial regions is believed to have led to the loss of calcareous algae, decreased body-size in marine invertebrates and to a near-absence of fishes in these areas (Sun *et al.* 2012). A later study has recorded actinopterygian predator fishes of the genera *Birgeria* and *Saurichthys* in LSTM strata in Nevada at ~20° N, indicating that at least some low latitudinal areas were inhabitable (Romano *et al.* 2017).

In northern middle latitudes, such as North Greenland, Spitsbergen and the Barents Sea area, the presence of ammonoids indicates that the upper water column was, at least at times, habitable during the LSTM (this study and Vigran *et al.* 1998, 2014; Galfetti *et al.* 2007b). However, the general lack of bioturbation in the laminated Smithian beds in North Greenland, with only rare occurrences of *Planolites* and possible *Zoophycos* at some levels, indicates that bottom conditions were unfavourable to benthic organisms during the LSTM. Bioturbation appears restricted to beds interpreted as storm deposits. The presence of pyrite may indicate anoxic or euxinic conditions, but the very low TOC values (0.2–0.3 wt %) suggest limited production of organic material as well as limited transport of organic matter to the basin and subsequently limited burial of organic matter. Interestingly, phytoplankton abundance (acritarchs and prasinophytes) is also very low, generally around 10 % or less. In Spitsbergen, storm beds are rare in LSTM strata (Wignall *et al.* 2016). The upper Smithian Mineral Mountains strata in Utah contain frequent storm-induced deposits in an upper offshore setting, where bioturbation appears to be restricted to these storm beds (Thomazo *et al.* 2019).

The hot temperatures on land during the LSTM are believed to have led to a diversity minimum amongst vertebrates and to the extirpation of *Lystrosaurus* (Fröbisch *et al.* 2010), and widespread decline in gymnosperm vegetation (Sun *et al.* 2012). Extreme temperatures over land, in excess of 35 °C, favouring photorespiration over photosynthesis, was suggested to have driven most terrestrial plants out of the equatorial areas (Sun *et al.* 2012).

During Early Triassic time terrestrial red beds were widespread, indicating at least seasonal arid to semi-arid conditions prevailed

in these areas (Table 2; Fig. 8a). Close to the equator in the Northern Hemisphere, sedimentary LSTM successions in Iberia between 10° and 14° N consist of conglomerates and aeolian sand dunes with rare occurrences of unconfined flash flood beds, testifying to arid conditions in near-equatorial areas (Borruel-Abadia *et al.* 2015). Arid to semi-arid conditions also prevailed in large parts of the Central European Basin at 20–30° N, and East Greenland at 30–40° N (Clemmensen, 1980; Preto *et al.* 2010; Kustatscher *et al.* 2014; Radley & Coram, 2016). In the Southern Hemisphere, red beds and arid to semi-arid conditions have been reported from Antarctica at 60° S, India at 45–60° S and South Africa at 40–60° S (Casshyap, 1979; McLoughlin *et al.* 1997; Neveling, 2004; Lindström & McLoughlin, 2007). Both sedimentological and ichnological data suggest that the Smithian of South Africa was characterized by prolonged intervals of drought alternated with brief periods of floods (Bordy & Krummeck, 2016). The evapotranspiration rate is believed to have greatly outpaced the rate of precipitation, and the fluvial systems may have been non-perennial (Neveling, 2004).

In the north, in Peary Land, the xerophytic lycopsid spore *Densoisporites nejburgii* is only abundant in the Smithian, where it constitutes at least ~30 % of the spore-pollen flora in Dunken-2 and 15–35 % at Hjulspordalen, while bisaccate pollen constitute ~20 % and ~20–30 % at these localities, respectively (Figs 2, 3). A similar pattern was recorded in the Barents Sea where Smithian assemblages are composed of between 80 and 90 % spores, and *D. nejburgii* also constitutes up to 30 % of the palynoflora (Galfetti *et al.* 2007b; Hochuli & Vigran, 2010). Hochuli & Vigran (2010) argued that *Aratrisporites* spp. and *D. nejburgii* had different ecological preferences, and that the former was hygrophytic in contrast to the latter. However, their quantitative data show the two taxa following a similar overall pattern (Galfetti *et al.* 2007b). These authors considered the late Smithian in the Barents Sea area to have been an interval with fairly stable humid conditions that favoured growth of hygrophytic floral elements.

In NW and Central Europe, *D. nejburgii* is generally one of the dominant elements in Smithian strata (Kürschner & Herngreen 2010), but quantitative assessments are rarely reported. High abundances of *D. nejburgii* would be expected if this taxon was xerophytic, and this seems to be the case. Middle Buntsandstein palynofloras from southeastern Poland were assigned to the *nejburgii* Subzone by Fijałkowska-Mader (1999). These assemblages were dominated by ~52–70 % spores, primarily *Densoisporites nejburgii* and *D. playfordii*. Corresponding *nejburgii* Zone assemblages from Germany consisted of ~98% spores (Fijałkowska-Mader, 1999). These palynofloras were preceded by assemblages with high abundances of acritarchs in the lower Middle Buntsandstein (Fijałkowska-Mader, 1999). In the Netherlands, Smithian palynofloras were dominated by *D. nejburgii* together with a variety of other lycopsid spore taxa, together with *Lunatisporites noviaulensis*, and were interpreted as pioneering vegetation on relatively dry and well-drained flood plains (Van der Zwan & Spaak, 1992).

In the Southern Hemisphere, close to the equator, biomarker data from South China indicate a dominance of spore-producing plants during Smithian times (Saito *et al.* 2013). The biomarkers retene, simonellite and dehydroabietane, which can be derived from multiple plant groups, including conifers, lycopsids and/or herbaceous bryophytes, were relatively abundant during the Smithian in South China (Fig. 7). Saito *et al.* (2013) interpreted the abundance of these biomarkers together with relatively low

Table 2. Summary of terrestrial climate indications from the Smithian–lower Anisian

Number on Fig. 8.	Locality	Latitude	The Late Smithian Thermal Maximum	The Smithian–Spathian cooling	Early Spathian	Middle–Late Spathian	Early Anisian
2	Barents Sea, Svalis Dome[1]	45° N	Deforested, dry, *D. nejburgii* = 30 %	Forestation, seasonally, semi-dry, *D. nejburgii* = 16 %	Forests, seasonally semi-dry, *D. nejburgii* <15 %	Forests, scattered, seasonally dry, *D. nejburgii* >40 % in middle Spathian, to <20 % in late Spathian	-
3	Peary Land[2]	45° N	Deforested, dry, *D. nejburgii* = 30 % Storms	Forestation, *D. nejburgii* = 0 %	Forests, *D. nejburgii* <1 %	Forests, scattered, *D. nejburgii* <1 %	Forests, *D. nejburgii* = 0 %
5	East Greenland[3]	35° N	Arid to semi-arid, red beds, arkoses, conglomerates	Arid to semi-arid, red beds, arkoses, conglomerates	Arid to semi-arid, red beds, arkoses, conglomerates	Arid to semi-arid, red beds, arkoses, conglomerates	Arid to semi-arid, red beds, arkoses, conglomerates
6, 7, 8	The Netherlands,[4] Poland,[5,6] Germany[5,6,7,22]	25–30° N	Deforested, dry, *D. nejburgii* abundant	Deforested, dry, *D. nejburgii* present, an increase in hygrophytic spores	Deforested, dry, *D. nejburgii* present, an increase in hygrophytic spores	Deforested, dry, *D. nejburgii* common, an increase in hygrophytic spores	Forestation, semi-arid, increase in gymnosperms, *D. nejburgii* disappears.
9, 10	Dolomites[7] and Hungary[8]	20° N	Deforested, dry, *D. nejburgii* abundant	-	Deforested, arid to semi-arid, *D. nejburgii* = 80–90 %	Forestation, *D. nejburgii* gradual decrease from 80 % to 0 %	Forestation, semi-arid, increase in gymnosperms *D. nejburgii* = 0 %
11	Iberia[9]	10–14° N	Arid, conglomerates, aeolian dunes, unconfined flash flood deposits	Semi-arid, fluvial sedimentation	Arid, aeolian dunes	Arid middle Spathian. Increased humidity in late Spathian sporadic plant and animal fossils	Semi-arid to arid, plant (conifers and sphenophytes) and tetrapod tracks
14	South China[10]	~0–5° S	Deforested, biomarker data	Forestation, biomarker data	Forested, biomarker data	Forested, biomarker data	-
16	Pakistan[11]	35° S	Deforested, semi-dry, *D. nejburgii* <10 %	Forestation, *D. nejburgii* <4 %	Deforestation, *D. nejburgii* <5–10 %	Deforestation, *D. nejburgii* = 0–11 %	Forestation, *D. nejburgii* = ~1 %
18	Tibet[12]	40° S	Deforested, *D. nejburgii* = 0 %	Forestation	Deforestation, *D. nejburgii* <1 %	-	-
17	Kenya[13]	40° S	Deforested, dry, *D. nejburgii* = 30 %	Forestation, *D. nejburgii* = 0 %	-	-	-
19	Madagascar[14]	45° S	Deforested, humid?, *D. nejburgii* = ?0 %	-	-	-	-
20	Carnarvon Basin[15,16]	50° S	Deforested, humid, *D. nejburgii* = 0 %	?	Forestation, bisaccates dominate	Forested, bisaccates dominate	Forested, bisaccates dominate
21	Perth Basin[17]	55° S	Deforested, humid, *D. nejburgii* = 0 %	-	-	-	-
23	Prince Charles Mountains[18,19]	60° S	Arid to semi-arid, red beds	Arid to semi-arid, red beds	Arid to semi-arid, red beds	Arid to semi-arid, red beds	Arid to semi-arid, red beds
24	Eastern Australia, Sydney Basin[20]	65–70° S	Deforested, *D. nejburgii* = very abundant (~30–50 %) CIA = ~75	Forestation, *D. nejburgii* = ~20 %, increased humidity, CIA = ~95	Deforested, seasonally humid, *D. nejburgii* <5 % CIA = ~95	Deforested, seasonally humid, *D. nejburgii* = ~10 % CIA = ~95	Deforested, seasonally humid, *D. nejburgii* < 5%
25	Central Transantarctic Mountains[21]	80° S	Forests, seasonally humid	Forests, seasonally humid	Forests, seasonally humid	Forests, seasonally humid	Forests, seasonally humid

After: 1 – Galfetti *et al.* (2007b); 2 – this work; 3 – Clemmensen (1980); 4 – Van der Zwan & Spaak (1992); 5 – Fijałkowska (1994); Fijałkowska-Mader (1999); 6 – Orlowska-Zwolińska (1984); 7 – Kürschner & Herngreen (2010); 8 – Looy *et al.* (1999); 9– Borruel-Abadia *et al.* (2015); 10 – Saito *et al.* (2013); 11 – Hermann *et al.* (2012b); 12 – Schneebeli-Hermann *et al.* (2015); 13 – Hankel (1991); 14 – Hankel (1993); 15 – Balme (1963); 16 – Dolby & Balme (1976); 17 – Haig *et al.* (2015); 18 – McLoughlin *et al.* (1997); 19 – Lindström & McLoughlin (2007); 20 – Fielding *et al.* (2019); 21 – Escapa *et al.* (2011); 22 – Kustatscher *et al.* (2014).
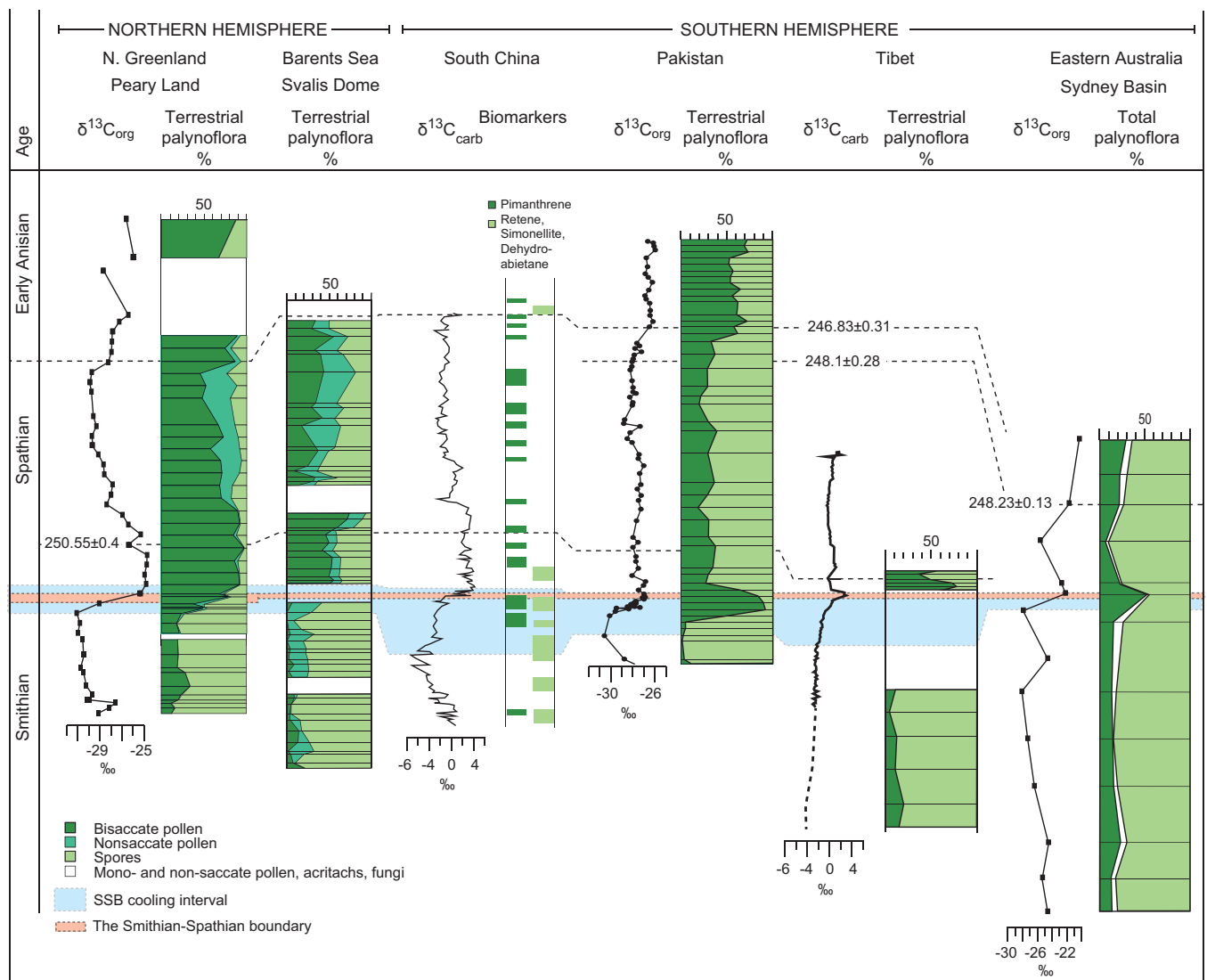
Fig. 7. Correlation between terrestrial palynofloras in the Northern Hemisphere: Peary Land (this work) and the Barents Sea (Galfetti *et al.* 2007*b*); and the Southern Hemisphere: biomarker data from South China (Saito *et al.* 2013); palynology from Pakistan (Hermann *et al.* 2012*b*), Tibet (Schneebeli-Hermann *et al.* 2012) and eastern Australia (Fielding *et al.* 2019).

C/N ratio values as an indication that these biomarkers were derived from herbaceous lycopsids and/or bryophytes. In the lower mid-latitudes at ~35° S, Tethyan assemblages from Pakistan are dominated by hygrophytic lycopsid spores assigned to *Lundbladispora* spp. and *Densoisporites* spp. (Hermann *et al.* 2012*b*; Romano *et al.* 2013). In the late Smithian period *Densoisporites* spp. becomes totally dominant composing >80 % of the assemblages, but *D. nejburgii* never composes more than 10 % of the palynoflora (Hermann *et al.* 2012*b*). In Tibet, at ~40° S, the Smithian assemblages are also dominated by cavate spores assigned to *Lundbladispora* spp. and *Densoisporites* spp., although *D. nejburgii* was not recorded (Schneebeli-Hermann *et al.* 2012). Further to the west, at ~45° S, age-equivalent spore-pollen assemblages reported from the Majunga Basin on Madagascar are composed of ~87 % spores, with an average of 30 % *D. nejburgii* (Hankel, 1993).

In Western Australia, located at ~50–55° S, Smithian strata belong to the *Protohaploxypinus samoilovichii* Zone (Haig *et al.* 2015), but were originally assigned to the *Kraeuselisporites saeptatus* Zone

Balme (Balme, 1963; Dolby & Balme, 1976). In the Perth Basin, assemblages from the Kockatea Shale assigned to the *Protohaploxypinus samoilovichii* Zone are 80–95 % dominated by spores, primarily *Densoisporites playfordii* and *Kraeuselisporites saeptatus* (Balme, 1963; Haig *et al.* 2015). The Kockatea Shale probably represents the southernmost deposition of marine strata within the East Gondwana rift that stretched southwest along the western margin of present-day Australia into the interior of Gondwana (Harrowfield *et al.* 2005). The Kockatea Shale is interpreted as having been deposited in a shallow interior sea, with variable estuarine water conditions, and subjected to ephemeral or otherwise harsh conditions. In the Prince Charles Mountains in Antarctica, at ~60° S, located further inland within the East Gondwana rift, Lower Triassic variegated beds assigned to the *Lunatisporites pellucidus* Zone were replaced by red beds indicating predominantly arid conditions during Early Triassic time (McLoughlin *et al.* 1997; Lindström & McLoughlin, 2007). In the Sydney Basin (eastern Australia) located at ~65–70° S, zonate trilete spores constitute up to 54 % of the total palynoflora in the middle to upper Smithian, and a majority of these

spores can be attributed to *D. nejburgii* or the morphologically similar *D. solidus* Segroves, 1970 (Fielding *et al.* 2019; C. Mays, pers. comm. 2019). The chemical index of alteration (CIA = ~75) indicates less intense alteration of feldspars to clay minerals, and thus less intense weathering at this time, compared to in succeeding strata (Fielding *et al.* 2019). In the far south, at ~80° S, probable Smithian–Spathian strata from the Transantarctic Mountains contain a low-diversity flora, interpreted to have grown under seasonally wet conditions, including the corystospermous seed fern *Dicroidium zuberi* and the voltzialean conifers *Voltziopsis africana* and *V.* sp. cf. *angusta* and very few other elements (Escapa *et al.* 2011).

Thus, it indeed seems as if spore-producing plants were dominant globally during Smithian time. Gymnosperms were present, but in low numbers, and more forested areas seem to have been located along the southern Tethyan coast, Panthalassa and in the high southern latitudes (Fig. 8). In contrast to bisaccate pollen, which are mainly distributed by wind, spores are shed close to the parent plant and are thus primarily distributed into the marine environment via rivers. It is further important to note that there is a high probability that the gymnosperms produced higher amounts of pollen, compared to spore-producing plants. This makes the high abundance of spores globally during Smithian time even more remarkable.

Sun *et al.* (2012) suggested that high temperature was the cause of the repression of gymnosperms, but also noted that this would require air temperatures up to or above 35 °C. The occurrence of red beds in low latitudes, in high latitudes in the Southern Hemisphere and in mid-latitudes in the Northern Hemisphere, attests to predominantly hot temperatures globally on land. This could explain why gymnosperm vegetation was suppressed to high latitudes (~80° S) in the Southern Hemisphere (Fig. 8). Repeated prolonged dry seasons would not be able to sustain trees and wet-loving ferns over large lowland areas. These plants would be restricted to wetter environments along rivers and lake margins. In accordance with VanBuren *et al.* (2018), who found that the lycophyte *Selaginella lepidophylla* could be desiccated to only 10 % of its water content for three years, and thereafter revived, prolonged drought during the LSTM would favour herbaceous drought-tolerant plants, e.g. the *Pleuromeia* that produced *Densoisporites nejburgii*. Brief wet seasons during the LSTM would allow fast regrowth of herbaceous lycopsid plants on the lowland areas as well as mass transport of spores to the basin during the wetter season. Under climatic conditions with recurrent prolonged dry intervals, woody plants that have much longer generation cycles than herbaceous spore-producing plants would perish or be suppressed to localized 'humid spots'.

5.b. The Smithian–Spathian cooling interval

The SSB cooling interval is herein defined as the interval between the late Smithian minimum C-isotope value and the first early Spathian maximum in $\delta^{13}C$. During this interval, the palynological assemblages from the Dunken-2 core are dominated by unidentified palynomorphs, which increased in abundance already in the uppermost LSTM sample. The increase in unidentified palynomorphs may be linked to a marked increase in burrowing activity during the Smithian–Spathian cooling interval, which indicates that bottom conditions had improved so that benthic organisms could thrive. In contrast, acritarchs never exceed 10 % of the total assemblage and appear to decline in abundance, and no ammonoids were recovered from this interval. Bisaccate pollen appear to increase gradually in concert with the increasing $\delta^{13}C$-values (Fig. 2).

The difference in palynofloral composition between Peary Land and Svalis Dome (Galfetti *et al.* 2007b), both situated at ~45° N, suggests a difference in vegetation on the eastern and western coasts of the Barents Sea at this time (Fig. 7). To the west, in Peary Land, the gradual replacement of herbaceous vegetation with gymnosperms occurs without major incorporation of ginkgos/cycads, while to the east (Svalis Dome), the latter group constitute most of the corresponding initial reduction in herbaceous plants (Fig.7). This may indicate that seasonally drier conditions continued to prevail to the east of the Barents Sea. This is also suggested by *Densoisporites nejburgii*, which accounts for ~16 % of the spores (mean value; (Galfetti *et al.* 2007b) in the Svalis Dome record, while it was not recorded within this interval in Peary Land.

In Iberia, at 10–14° N, semi-arid conditions with primarily fluvial deposition prevailed (Borruel-Abadia *et al.* 2015). In Utah, at 10° N, the Smithian–Spathian cooling is associated with a cessation of frequent storm beds with associated bioturbation (Thomazo *et al.* 2019). This shift takes place during a maximum flooding and deepening of the depositional setting to lower offshore (Thomazo *et al.* 2019).

Correlation of the Smithian–Spathian cooling interval from the Northern to the Southern Hemisphere indicates that there might be a slight difference in timing of the vegetation responses between these areas (Fig. 7). In Greenland, the gradual increase in gymnosperm pollen in North Greenland coincides with the gradual increase in $\delta^{13}C$ and reaches a maximum when the $\delta^{13}C$ also reaches a maximum. In Pakistan the change appears to commence slightly earlier, while $\delta^{13}C$-values are still very low and in addition, the maximum abundance of gymnosperm pollen is reached prior to the maximum $\delta^{13}C$-value (Fig. 7). This also seems to be the case in Tibet and in eastern Australia (Fig. 7). Similar to the Greenland record, *D. nejburgii* rarely constitutes more than a couple of per cent of the spore-pollen flora in Pakistan during the Smithian–Spathian cooling (Hermann *et al.* 2012b). In South China the gymnosperm biomarker pimanthrene is first recorded from the uppermost Smithian, and co-occurs with biomarkers interpreted as indicating herbaceous plants (Saito *et al.* 2013). The appearance of pimanthrene precedes the most pronounced increase in $\delta^{13}C_{carb}$-values (Fig. 7). A palynoflora from Kenya, at ~40° S, assigned to the *Protohaploxypinus samoilovichii* Zone is dominated by ~52 % bisaccate pollen (Hankel, 1991). This probably represents the cooling interval (Fig. 7). Spores make up ~44 % and *D. nejburgii* was not registered (Hankel, 1991). In the lowermost part of the *Aratrisporites tenuispinosus* Zone in the Sydney Basin, bisaccate pollen grains temporarily increase to 50 % and this coincides with a major increase in C-isotope values, and *Densoisporites nejburgii*-type spores are still common making up <20 % of the total palynoflora (Fielding *et al.* 2019); C. Mays pers. comm. 2019). The CIA is increased (~95), indicating more intense alteration of feldspars, hence, stronger weathering than during Smithian time (Fielding *et al.* 2019).

From the spore-pollen records, it appears as if conditions became more favourable for gymnosperms earlier in the mid-southern latitudes than in the mid-northern latitudes where the vegetation response was delayed. The global forestation at the SSB would help draw down CO_2 from the atmosphere, accelerating the global cooling.

5.c. The early Spathian $\delta^{13}C$ maximum

In Peary Land, at ~45° N, early Spathian organic C-isotope values remain relatively stable during early Spathian time, varying between

(a) Late Smithian Thermal Maximum

(d) Base map with localities

Localities:
1. Svalbard, Norway
2. Barents Sea, Norway
3. Peary Land, Greenland
4. Sverdrup Basin, Arctic Canada
5. East Greenland
6. Poland
7. Germany
8. The Netherlands
9. Dolomites
10. Hungary
11. Iberia
12. Nevada, USA
13. Sonora Foreland Basin, USA
14. South China
15. Zal, Iran
16. Pakistan
17. Kenya
18. Tibet
19. Majunga Basin, Madagascar
20. Carnarvon Basin, Western Australia
21. Perth Basin, Western Australia
22. Karoo Basin, South Africa
23. Prince Charles Mountains, Antarctica
24. Sydney Basin, eastern Australia
25. Central Transantarctic Mountains, Antarctica

Red beds, aeolian dunes

Spore dominated

Gymnosperm pollen dominated

Deep ocean

Shallow ocean

Land

Mountains

E<P   Evaporation < Precipitation

E>P   Evaporation > Precipitation

E>>P   Evaporation >> Precipitation

(b) Smithian-Spathian cooling
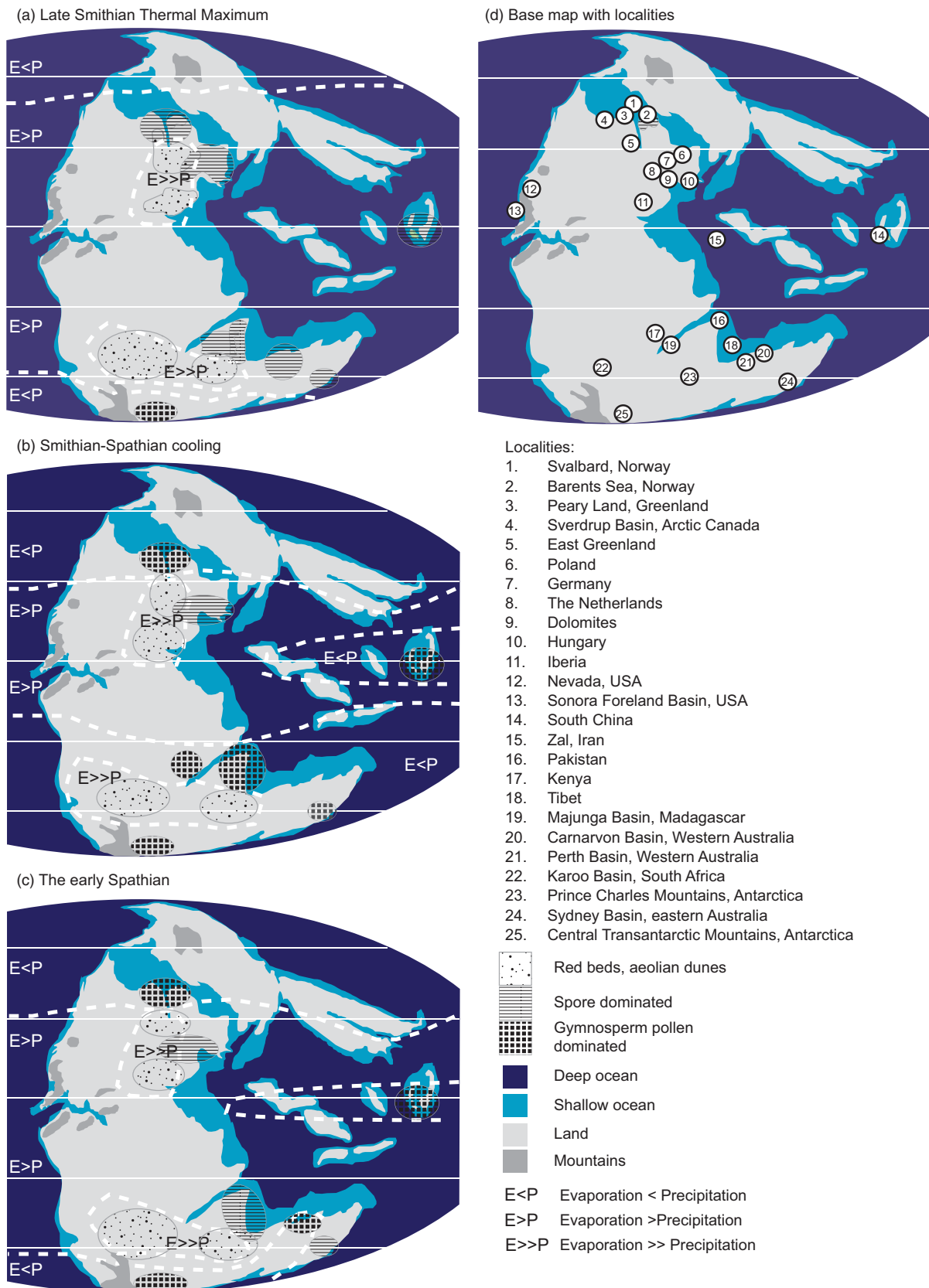
(c) The early Spathian

Fig. 8. Palaeogeographical maps of Pangaea showing dominant vegetation as inferred from previous published palynological and palaeobotanical records and our new data from North Greenland, for (a) the Late Smithian Thermal maximum; (b) the Smithian–Spathian cooling interval; and (c) the early Spathian C-isotope maximum. The palaeomap reconstructions are modified from Schneebeli-Hermann *et al.* (2015). Palynological, palaeobotanical and sedimentological references can be found in the main text, and many are listed in Table 2.

−25 ‰ and −24.5 ‰ (Figs 2, 7). Pyrite was registered at some levels, but trace fossils are common. In the lowermost part, acritarchs are either absent or rare, and the amount of unidentified palynomorphs is high but decreases rapidly upsection (Fig. 2). In the succeeding samples acritarchs increase markedly, fluctuate and occasionally reach 50 % of the total assemblage. The maximum $\delta^{13}C$-values coincide with a palynoflora dominated by almost 90 % bisaccate pollen. *Densoisporites nejburgii* was not registered in the lower Spathian of the Dunken-2 core, but this may be due to the generally poor preservation and high maturity of the organic material. It was recorded in the more well-preserved assemblages from Hjulspordalen, but in very low numbers, <1 % of the spore-pollen flora. In the Barents Sea area, on the other hand, *D. nejburgii* remains a common element in the lower Spathian, commonly making up ~2–8 % of the palynoflora, rarely exceeding 15 % (Galfetti *et al.* 2007b). In addition, bisaccate pollen only constitute 55–60 % of the palynoflora in the lower Spathian (Galfetti *et al.* 2007b), indicating regional differences within the Barents Sea, between the Svalis Dome area to the east and Peary Land to the west (Fig. 7). A comparison with the composite $\delta^{13}C_{carb}$-record from China, which has been age constrained by U–Pb ages from ash beds (Galfetti *et al.* 2007a), shows that the early Spathian $\delta^{13}C$ maximum lasted until 250.55 ± 0.40 Ma (Ovtcharova *et al.* 2006), after which C-isotope values again began to decrease. The late early Smithian $\delta^{13}C_{org}$-record from Peary Land follows the same trend, decreasing gradually and reaching less than −28 ‰ in the upper part of the *Pechorosporites disertus* Zone (Figs 2, 7). During the interval with steadily decreasing C-isotope values, the spore-pollen record remains fairly stable, with a total dominance of bisaccate pollen (Fig. 7). The palynoflora does not show any obvious response to the decreasing C-isotope values (Figs 2, 7).

In East Greenland, at ~35° N, arid to semi-arid conditions appear to have continued to prevail (Clemmensen, 1980). Further south, in the Netherlands at ~25° N, Spathian palynofloras are characterized by in principle the same palynofloral elements as during Smithian time, but with an increase in hygrophytic spores, and were interpreted as representing moderately dry climatic conditions during Spathian time (Van der Zwan & Spaak, 1992). In Hungary, at ~20° N, *D. nejburgii* composed almost 90 % of the spore-pollen flora at this time (Looy *et al.* 1999), demonstrating that semi-arid conditions still prevailed. In Iberia, at ~10–14° N, arid conditions with sand dunes dominated (Borruel-Abadia *et al.* 2015).

In the Southern Hemisphere, in South China at ~0–5° S, biomarker data suggest that gymnosperms continued to thrive while herbaceous plants only played a minor role (Saito *et al.* 2013). In Pakistan, at ~35° S, the gymnosperm-dominated assemblages were again replaced by spore-dominated palynofloras already during the early Spathian $\delta^{13}C$ maximum (Hermann *et al.* 2012b). Bisaccate pollen decreased to between 30 and 40 % prior to a stratigraphic level correlated with a 250.55 ± 0.40 Ma age by Ovtcharova *et al.* (2006) as extrapolated by Hermann *et al.* (2012a) (Fig. 7). Thus, the change from bisaccate-dominated to yet again spore-dominated microfloras appears to take place prior to a minor shift to more negative C-isotope values (Hermann *et al.* 2012a) (Fig. 7). *Densoisporites nejburgii* is generally absent or composes <5 % of the palynoflora, except towards the top of the interval where it occasionally reaches ~10 % (Hermann *et al.* 2012b). The recurrent Spathian spore dominance in the Pakistan record was interpreted to indicate increased humidity (Hermann *et al.* 2012a). In the early Spathian palynoflora from Tibet, at ~40° S, *D. nejburgii* occurs in very low numbers in assemblages dominated by bisaccate pollen, *Densoisporites* spp. and *Aratrisporites* spp. (Schneebeli-Hermann

et al. 2012). In eastern Australia, palynofloras with a 50/50 abundance between spores and bisaccates was replaced by assemblages containing ~70 % spores, but in which *D. nejburgii* played a very subordinate role (Fielding *et al.* 2019; Fig. 7). Hence, while gymnosperms thrived in mid-latitudes of the Northern Hemisphere during early Spathian time, they only appear to have played a significant role during the earliest Spathian in the mid-latitudes of the Southern Hemisphere (Table 2; Fig. 7). In high-latitude areas like the Transantarctic Mountains, at ~80° S, gymnosperm forests continued to prevail (Escapa *et al.* 2011), but these were likely separated from mid-latitudinal areas by a semi-arid belt stretching from the Prince Charles Mountains to South Africa (McLoughlin *et al.* 1997; Neveling, 2004) (Fig. 8).

5.d. The middle to late Spathian and Spathian–Anisian boundary

In Peary Land the C-isotope values become more negative until they appear to stabilize just above −30 ‰ in the middle part of the *Jerseyiaspora punctispinosa* Zone (Figs 2, 7). Middle Spathian strata are interpreted as having been deposited closer to the coast, but the acritarch abundance remains relatively high, varying between 20 and 50 % of the total assemblages. During this interval the spore abundance remains fairly stable, but bisaccate pollen decrease on behalf of non-saccate grains, primarily *Monosulcites* spp., signalling establishment of a mixed flora containing conifer and corystosperm trees, along with ginkgo/cycads, lycophytes and ferns. Monosulcate grains were already present during the Smithian, but never abundant. The overall pattern is similar in the Barents Sea, with the difference that there *D. nejburgii* is abundant in middle Spathian (>20 % to <40 %) assemblages (Galfetti *et al.* 2007b), while it is virtually absent in Peary Land. In addition, non-saccate pollen appears to have played a more significant role throughout the Smithian–Spathian interval in the Svalis Dome area, again signalling some difference in vegetation on either side of the Barents Sea (Figs 7, 8).

Around the Spathian–Anisian boundary, $\delta^{13}C$ values again turn more positive to around −28 ‰ in the North Greenland record, and this change is again in concert with an increase in bisaccate pollen (Fig. 7). In Peary Land this occurs within an interval of lower to upper shoreface sandstones, from which only sparse palynofloras were recovered (Fig. 2). The early Anisian assemblages from Peary Land contain fairly high amounts of acritarchs, ~20 % in Dunken-2, between 30 and 40 % in the Dunken-2B core and between 30 and 80 % at Hjulspordalen (Figs 2, 3). Bioturbation indices of between 3 and 5 indicate oxygenated conditions, and the presence of ammonoids (of the *Lenotropites caurus* Zone) suggests habitable conditions in the upper water column (Figs 2, 3). The spore-pollen flora is dominated by bisaccate pollen indicating the presence of forests on land (Fig. 7).

In NW Europe, at ~25–30° N, the early Anisian period is characterized by the appearance of a new suite of gymnosperm pollen, with *Triadispora* spp. and *Protodiploxypinus* spp. becoming dominant. At this time *D. nejburgii* disappears and is replaced by members of *Aratrisporites* spp. (Kürschner & Herngreen, 2010). In Hungary, at ~20° N, *D. nejburgii* gradually decreases in abundance during middle to late Spathian times and disappears around the Spathian–Anisian boundary (Looy *et al.* 1999). Contemporaneous forest development appears to have taken place in steps during middle–late Spathian times, but in early Anisian time gymnosperms completely dominate the spore-pollen flora (Looy *et al.* 1999).

In the Southern Hemisphere, the conditions during middle and late Spathian times were very similar to during early Spathian time (Table 2). In southern China (Fig. 7), at ~0–5° S, biomarker data indicate continued dominance of gymnosperms during middle to late Spathian times (Saito *et al.* 2013).

Spore-producing plants appear to continue to dominate through the middle and upper Spathian in the Pakistan record, at ~35° S, but in early Anisian time there is a shift to a more gymnosperm-dominated flora signalling a return of forests on land (Fig. 7). In the Carnarvon Basin, Western Australia, at ~50° S, palynofloras from the Spathian–lower Anisian are stated to be dominated by non-taeniate bisaccate pollen grains, primarily *Falcisporites* spp. and *Alisporites* spp., thus indicating the establishment of forests already from middle Spathian time (Dolby & Balme, 1976). In eastern Australia, at ~65–70° S, palynofloral records indicate a slight increase in gymnosperm pollen during the middle to upper Spathian and lowermost Anisian, but spores still dominate and *D. nejburgii* composes <10 % (Fielding *et al.* 2019; C. Mays pers. comm. 2019). In the far south of the Transantarctic Mountains, at ~80° S, seasonally humid forests continued to prevail (Escapa *et al.* 2011).

5.e. The link between δ¹³C$_{org}$ and terrestrial vegetation

Overall the general composition of Smithian–early Anisian spore-pollen floras appear to mirror changes in $\delta^{13}C$ (Fig. 7). In particular, the abundance of bisaccate gymnosperms appear to reflect the C-isotope variations, with only some minor deviations in timing in the lower Spathian of Peary Land and in the Smithian–lower Spathian in Pakistan (Fig. 7). This may reflect the influence arborescent vegetation has on the carbon cycle. Today, ~30 % of the Earth's surface is covered by forest ecosystems, and these may sequester as much as 25 % of anthropogenic carbon emissions (Anderegg *et al.* 2013). In accordance with climate-vegetation modelling (Anderegg *et al.* 2013), the global warming that led to the LSTM would have caused widespread drought-induced tree mortality and rapid species range contraction. The deforestation would exacerbate global warming by substantially increasing carbon emissions from dead and decomposing trees (Hicke *et al.* 2012). Deforestation would increase near-ground solar-radiation, which would affect understorey plants and nutrient cycling (Anderegg *et al.* 2013). However, exposure of previously forested land areas, especially desertification, would also affect the albedo of the disturbed areas. Normally an increase in albedo over land is considered to cause warming when other parameters are not considered, but coupled land–ocean–atmosphere modelling instead shows that global deforestation, where forests are replaced by grasslands, instead lead to a net global cooling of −1 °C (Davin & de Noblet-Ducoudre, 2010). This is mainly because the albedo effect spreads over the ocean, while the other effects (evapotranspiration and surface roughness) do not (Davin & de Noblet-Ducoudre, 2010). However, the effect over the continents will vary from equator to pole as the balance between the different processes depends on the latitude. With the present-day geography, the albedo effect is stronger in the boreal and temperate zones in the Northern Hemisphere, where land area is larger than in the Southern Hemisphere, and will therefore induce cooling. The net cooling will be strongest in areas north of 40° N, from between 2− °C and as much as −4.2 °C at latitudes 70–80° N (Davin & de Noblet-Ducoudre, 2010). In the tropics, however, the net cooling will be minimal <1 °C (Davin & de Noblet-Ducoudre, 2010).

Thus, the deforestation and desertification during the LSTM could ultimately have contributed to global cooling. The cooling effect over land would have been stronger in the mid- and high latitudes, especially in the Southern Hemisphere, than in the tropics, as the Southern Hemisphere held more land area than the Northern Hemisphere. This may explain why recovery of gymnosperm vegetation began earlier in the mid-latitudes of Pakistan than in Peary Land in the Northern Hemisphere (Fig. 7).

A dramatic decrease in weathering intensity across the SSB has been inferred based on detrital proxy data from South China (Zhang *et al.* 2015). Based on the terrestrial palynofloral records, we propose that weathering was facilitated during the LSTM when conditions were hot and large land areas may have been exposed or only covered by herbaceous vegetation that could survive long periods of drought. However, during the LSTM erosion and transportation of sediments to the oceans would have been confined to sporadic episodes or brief wet seasons. Because of the lack of vegetation with deep roots, episodic high precipitation events would flush large amounts of weathered material to the basins. This is in accordance with Van der Zwan & Spaak (1992), who interpreted monsoonal activity under sea level highstands to have been responsible for activation of an ephemeral drainage system on the northern side of the Central European Highland during Smithian–early Spathian times, and that these changes in the drainage system led to mass transport of erosional products into NW Europe. The subsequent decrease in weathering across the SSB in the tropics could thus well be an effect of densification of vegetation and root systems. The compilation of palynological, palaeobotanical and sedimentological data in Table 2 accentuates the stark contrast between the near-global deforestation during the LSTM and the return of gymnosperm forests during the Smithian–Spathian cooling interval.

6. Conclusion

New δ¹³C$_{org}$ and spore-pollen records from Smithian–lower Anisian strata in Peary Land, North Greenland, constrained by palynology and ammonite biostratigraphy, allow for a re-evaluation of the global climatic changes from the LSTM through the Smithian–Spathian cooling interval and through the Spathian and Anisian periods. The North Greenland succession was situated at ~45° N on the northern margin of Pangaea, and shows a remarkable shift from spore-dominated assemblages during the LSTM to gymnosperm-dominated ones in early Spathian – early Anisian times. The LSTM is one of the most extreme global warming episodes of the Mesozoic Era, believed to have resulted in extreme temperatures in the equatorial upper ocean and on land. The LSTM is followed by a rapid cooling across the SSB globally and a shift to positive C-isotope values in early Spathian time. Correlations with other SSB successions with records of terrestrial floral change in the Barents Sea, Europe, Pakistan, Tibet, South China, Australia and Antarctica show that the recovery of gymnosperms began earlier in the mid-latitudes of the Southern Hemisphere (Pakistan) than in mid-latitudes on the Northern Hemisphere. Taking both the spore/bisaccate pollen ratios and the abundances of the xerophytic lycopsid spore *D. nejburgii* in different areas globally into account instead suggests that the LSTM was indeed hot, but also dry. Prolonged droughts combined with extreme heat during the LSTM would favour drought-tolerant and fast-growing spore-producing plants with fast generation shifts that could take advantage of episodic wet intervals over slow-growing gymnosperms with slow generation shifts that require

at least annual wet seasons. In accordance with modern coupled land–ocean–atmosphere modelling the near-global deforestation during the LSTM would increase the albedo and this would lead to a net global cooling, because the albedo effect spreads over the ocean, while the other effects (evapotranspiration and surface roughness) do not. The cooling effect would have been strongest in mid- to high latitudes, perhaps as much as −4 °C. The Smithian–Spathian cooling resulted in a change to a climate with seasonally more humid conditions primarily in mid-latitudes on both hemispheres. The recovery of gymnosperm vegetation facilitated drawdown of CO_2 from the atmosphere and further exacerbated cooling. However, mid-latitude areas in the Southern Hemisphere again experienced deforestation during early Spathian time, while in the Northern Hemisphere gymnosperms continued to be dominant. The correlation between the spore/bisaccate pollen ratio and shifts in $\delta^{13}C_{org}$ demonstrate the strong influence forests have on the carbon cycle and the global climate.

Author ORCIDs. 🄳 Sofie Lindström 0000-0001-8278-1055, Peter Alsen 0000-0001-6218-9054, Morten Bjerager 0000-0003-3180-8857, Hamed Sanei 0000-0002-2961-9654, Jørgen Bojesen-Koefoed 0000-0001-5647-2769

References

Anderegg WRL, Kane JM and Anderegg LDL (2013) Consequences of widespread tree mortality triggered by drought and temperature stress. *Nature Climate Change* **3**, 30–6.

Balme BE (1963) Plant microfossils from the Lower Triassic of Western Australia. *Palaeontology* **6**, 12–40.

Balme BE (1995) Fossil *in-situ* spores and pollen grains – an annotated catalog. *Review of Palaeobotany and Palynology* **87**, 81–323.

Bjerager M, Alsen P, Hovikoski J, Lindström S, Stemmerik L and Therkelsen J (In press) Triassic lithostratigraphy of the Wandel Sea Basin, North Greenland. *Bulletin of the Geological Society of Denmark*.

Bordy EM and Krummeck WD (2016) Enigmatic continental burrows from the early Triassic transition of the Katberg and Burgersdorp Formations in the main Karoo Basin, South Africa. *Palaios* **31**, 389–403.

Borruel-Abadia V, Lopez-Gomez J, De la Horra R, Galan-Abellan B, Barrenechea JF, Arche A, Ronchi A, Gretter N and Marzo M (2015) Climate changes during the Early–Middle Triassic transition in the E. Iberian plate and their palaeogeographic significance in the western Tethys continental domain. *Palaeogeography, Palaeoclimatology, Palaeoecology* **440**, 671–89.

Brayard A, Bucher H, Escarguel G, Fluteau F, Bourquin S and Galfetti T (2006) The Early Triassic ammonoid recovery: paleoclimatic significance of diversity gradients. *Palaeogeography, Palaeoclimatology, Palaeoecology* **239**, 374–95.

Brayard A, Escarguel G, Bucher H and Bruhwiler T (2009) Smithian and Spathian (Early Triassic) ammonoid assemblages from terranes: paleoceanographic and paleogeographic implications. *Journal of Asian Earth Sciences* **36**, 420–33.

Casshyap SM (1979) Patterns of sedimentation in Gondwana basins. In *Proceedings of the Fourth International Gondwana Symposium, Calcutta* (eds B Laskar and RCS Rao), pp. 525–51. Delhi: Hindustan Publishing Corporation.

Chen ZQ and Benton MJ (2012) The timing and pattern of biotic recovery following the end-Permian mass extinction. *Nature Geoscience* **5**, 375–83.

Chen ZQ, Tong JN and Fraiser ML (2011) Trace fossil evidence for restoration of marine ecosystems following the end-Permian mass extinction in the Lower Yangtze region, South China. *Palaeogeography, Palaeoclimatology, Palaeoecology* **299**, 449–74.

Clarkson MO, Richoz S, Wood RA, Maurer F, Krystyn L, McGurty DJ and Astratti D (2013) A new high-resolution delta C-13 record for the Early Triassic: insights from the Arabian Platform. *Gondwana Research* **24**, 233–42.

Clemmensen LB (1980) Triassic rift sedimentation and palaeogeography of central East Greenland. *Bulletin Grønlands Geologiske Undersøgelse* **136**, 1–72.

Davin EL and de Noblet-Ducoudre N (2010) Climatic impact of global-scale deforestation: radiative versus nonradiative processes. *Journal of Climate* **23**, 97–112.

Dickens GR, Oneil JR, Rea DK and Owen RM (1995) Dissociation of oceanic methane hydrate as a cause of the carbon-isotope excursion at the end of the Paleocene. *Paleoceanography* **10**, 965–71.

Dolby JH and Balme BE (1976) Triassic palynology of the Carnarvon Basin, Western Australia. *Review of Palaeobotany and Palynology* **22**, 105–68.

Droser ML and Bottjer DJ (1986) A semiquantitative field classification of ichnofabric. *Journal of Sedimentary Petrology* **56**, 558–9.

Escapa IH, Taylor EL, Cuneo R, Bomfleur B, Bergene J, Serbet R and Taylor TN (2011) Triassic floras of Antarctica: plant diversity and distribution in high paleolatitude communities. *Palaios* **26**, 522–44.

Fielding CR, Frank TD, McLoughlin S, Vajda V, Mays C, Tevyaw AP, Winguth A, Winguth C, Nicoll RS, Bocking M and Crowley JL (2019) Age and pattern of the southern high-latitude continental end-Permian extinction constrained by multiproxy analysis. *Nature Communications* **10**, 385. doi: 10.1038/s41467-018-07934-z.

Fijałkowska A (1994) Palynostratigraphy of the Lower and Middle Buntsandstein in north-western part of the Holy Cross Mts. *Geological Quarterly* **38**, 59–96.

Fijałkowska-Mader A (1999) Palynostratigraphy, palaeoecology and palaeoclimatology of the Triassic in south-eastern Poland. *Zentralblatt für Geologie und Paläontologie, I* **1998**, 601–27.

Fröbisch J, Angielczyk KD and Sidor CA (2010) The Triassic dicynodont *Kombuisia* (Synapsida, Anomodontia) from Antarctica, a refuge from the terrestrial Permian–Triassic mass extinction. *Naturwissenschaften* **97**, 187–96.

Galfetti T, Bucher H, Martini R, Hochuli PA, Weissert H, Crasquin-Soleau S, Brayard A, Goudemand N, Bruehwiler T and Guodun K (2008) Evolution of Early Triassic outer platform paleoenvironments in the Nanpanjiang Basin (South China) and their significance for the biotic recovery. *Sedimentary Geology* **204**, 36–60.

Galfetti T, Bucher H, Ovtcharova M, Schaltegger U, Brayard A, Bruhwiler T, Goudemand N, Weissert H, Hochuli PA, Cordey F and Guodun KA (2007a) Timing of the Early Triassic carbon cycle perturbations inferred from new U–Pb ages and ammonoid biochronozones. *Earth and Planetary Science Letters* **258**, 593–604.

Galfetti T, Hochuli PA, Brayard A, Bucher H, Weissert H and Vigran JO (2007b) Smithian–Spathian boundary event: evidence for global climatic change in the wake of the end-Permian biotic crisis. *Geology* **35**, 291–4.

Grasby SE, Beauchamp B, Bond DPG, Wignall PB and Sanei H (2016) Mercury anomalies associated with three extinction events (Capitanian Crisis, Latest Permian Extinction and the Smithian/Spathian Extinction) in NW Pangea. *Geological Magazine* **153**, 285–97.

Grasby SE, Beauchamp B, Embry A and Sanei H (2013a) Recurrent Early Triassic ocean anoxia. *Geology* **41**, 175–8.

Grasby SE, Sanei H, Beauchamp B and Chen ZH (2013b) Mercury deposition through the Permo-Triassic Biotic Crisis. *Chemical Geology* **351**, 209–16.

Grauvogel-Stamm, L. 1999. *Pleuromeia sternbergii* (Munster) Corda, eine charackteristische Pflanze des deutschen Buntsandsteins. In *Trias, Eine ganz andere Welt, Mitteleuropa im frühen Erdmittelalter* (eds N Hauschke and V Wilde), pp. 271–82. München: Pfeil.

Haig DW, Martin SK, Mory AJ, McLoughlin S, Backhouse J, Berrell RW, Kear BP, Hall RJ, Foster CB, Shi GR and Bevan JC (2015) Early Triassic (early Olenekian) life in the interior of East Gondwana: mixed marine–terrestrial biota from the Kockatea Shale, Western Australia. *Palaeogeography, Palaeoclimatology, Palaeoecology* **417**, 511–33.

Hankel O (1991) Early Triassic plant microfossils from the Kavee Quarry section of the Lower Mariakani Formation, Kenya. *Review of Palaeobotany and Palynology* **68**, 127–45.

Hankel O (1993) Early Triassic plant microfossils from Sakamena sediments of the Majunga Basin, Madagascar. *Review of Palaeobotany and Palynology* **77**, 213–33.

Harrowfield M, Holdgate GR, Wilson CJL and McLoughlin S (2005) Tectonic significance of the Lambert Graben, East Antarctica: reconstructing the Gondwanan rift. *Geology* **33**, 197–200.

Hermann E, Hochuli PA, Bucher H, Bruhwiler T, Hautmann M, Ware D, Weissert H, Roohi G, Yaseen A and Khalil ur R (2012a) Climatic oscillations at the onset of the Mesozoic inferred from palynological records from the North Indian Margin. *Journal of the Geological Society, London* **169**, 227–37.

Hermann E, Hochuli PA, Bucher H and Roohi G (2012b) Uppermost Permian to Middle Triassic palynology of the Salt Range and Surghar Range, Pakistan. *Review of Palaeobotany and Palynology* **169**, 61–95.

Hermann E, Hochuli PA, Mehay S, Bucher H, Bruhwiler T, Ware D, Hautmann M, Roohi G, ur-Rehman K and Yaseen A (2011) Organic matter and palaeoenvironmental signals during the Early Triassic biotic recovery: the Salt Range and Surghar Range records. *Sedimentary Geology* **234**, 19–41.

Hicke JA, Allen CD, Desai AR, Dietze MC, Hall RJ, Hogg EH, Kashian DM Moore D, Raffa KF, Sturrock RN and Vogelmann J (2012) Effects of biotic disturbances on forest carbon cycling in the United States and Canada. *Global Change Biology* **18**, 7–34.

Hochuli PA, Sanson-Barrera A, Schneebeli-Hermann E and Bucher H (2016) Severest crisis overlooked – worst disruption of terrestrial environments postdates the Permian–Triassic mass extinction. *Scientific Reports* **6**, 28372. doi: 10.1038/srep28372.

Hochuli PA and Vigran JO (2010) Climate variations in the Boreal Triassic – inferred from palynological records from the Barents Sea. *Palaeogeography, Palaeoclimatology, Palaeoecology* **290**, 20–42.

Horacek M, Koike T and Richoz S (2009) Lower Triassic delta C-13 isotope curve from shallow-marine carbonates in Japan, Panthalassa realm: confirmation of the Tethys delta C-13 curve. *Journal of Asian Earth Sciences* **36**, 481–90.

Horacek M, Richoz S, Brandner R, Krystyn L and Spotl C (2007) Evidence for recurrent changes in Lower Triassic oceanic circulation of the Tethys: the delta C-13 record from marine sections in Iran. *Palaeogeography, Palaeoclimatology, Palaeoecology* **252**, 355–69.

Håkansson E (1979) Carboniferous to Tertiary development of the Wandel Sea Basin, eastern North Greenland. *Grønlands Geologiske Undersøgelse, Report* **88**, 73–83.

Kaim A and Nutzel A (2011) Dead bellerophontids walking – the short Mesozoic history of the Bellerophontoidea (Gastropoda). *Palaeogeography, Palaeoclimatology, Palaeoecology* **308**, 190–9.

Komatsu T, Naruse H, Shigeta Y, Takashima R, Maekawa T, Dang HT, Dinh TC, Nguyen PD, Nguyen HH, Tanaka G and Sone M (2014) Lower Triassic mixed carbonate and siliciclastic setting with Smithian–Spathian anoxic to dysoxic facies, An Chau basin, northeastern Vietnam. *Sedimentary Geology* **300**, 28–48.

Komatsu T, Takashima R, Shigeta Y, Maekawa T, Tran HD, Cong TD, Sakata S, Dinh HD and Takahashi O (2016) Carbon isotopic excursions and detailed ammonoid and conodont biostratigraphies around Smithian–Spathian boundary in the Bac Thuy Formation, Vietnam. *Palaeogeography, Palaeoclimatology, Palaeoecology* **454**, 65–74.

Kustatscher E, Franz M, Heunisch C, Reich M and Wappler T (2014) Floodplain habitats of braided river systems: depositional environment, flora and fauna of the Solling Formation (Buntsandstein, Lower Triassic) from Bremke and Furstenberg (Germany). *Palaeobiodiversity and Palaeoenvironments* **94**, 237–70.

Kürschner WM and Herngreen GFW (2010) Triassic palynology of central and northwestern Europe: a review of palynofloral diversity patterns and biostratigraphic subdivisions. In *Triassic Timescale* (ed. SG Lucas), pp. 263–83. Geological Society of London, Special Publication no. 334.

Lindström S and McLoughlin S (2007) Synchronous palynofloristic extinction and recovery after the end-Permian event in the Prince Charles Mountains, Antarctica: implications for palynofloristic turnover across Gondwana. *Review of Palaeobotany and Palynology* **145**, 89–122.

Looy CV, Brugman WA, Dilcher DL and Visscher H (1999) The delayed resurgence of equatorial forests after the Permian–Triassic ecologic crisis. *Proceedings of the National Academy of Sciences of the United States of America* **96**, 13857–62.

McLoughlin S, Lindström S and Drinnan AN (1997) Gondwanan floristic and sedimentological trends during the Permian–Triassic transition: new evidence from the Amery Group, northern Prince Charles Mountains, East Antarctica. *Antarctic Science* **9**, 281–98.

Meyer KM, Yu M, Jost AB, Kelley BM and Payne JL (2011) delta C-13 evidence that high primary productivity delayed recovery from end-Permian mass extinction. *Earth and Planetary Science Letters* **302**, 378–84.

Neveling J (2004) Stratigraphic and sedimentological investigation of the contact between the Lystrosaurus and the Cynognathus Assemblage Zones (Beaufort group: Karoo Supergroup). *Council for Geoscience Bulletin* **137**, 1–164.

Orchard MJ (2007) Conodont diversity and evolution through the latest Permian and Early Triassic upheavals. *Palaeogeography, Palaeoclimatology, Palaeoecology* **252**, 93–117.

Orlowska-Zwolińska T (1984) Palynostratigraphy of the Buntsandstein in sections of western Poland. *Acta Palaeontologica Polonica* **29**, 107–17.

Ovtcharova M, Bucher H, Schaltegger U, Galfetti T, Brayard A and Guex J (2006) New Early to Middle Triassic U–Pb ages from South China: calibration with ammonoid biochronozones and implications for the timing of the Triassic biotic recovery. *Earth and Planetary Science Letters* **243**, 463–75.

Payne JL, Lehrmann DJ, Wei JY, Orchard MJ, Schrag DP and Knoll AH (2004) Large perturbations of the carbon cycle during recovery from the end-Permian extinction. *Science* **305**, 506–9.

Preto N, Kustatscher E and Wignall PB (2010) Triassic climates – state of the art and perspectives. *Palaeogeography, Palaeoclimatology, Palaeoecology* **290**, 1–10.

Radley JD and Coram RA (2016) The Chester Formation (Early Triassic, southern Britain): sedimentary response to extreme greenhouse climate? *Proceedings of the Geologists' Association* **127**, 552–7.

Retallack G (1975) The life and times of a Triassic lycopod. *Alcheringa* **1**, 3–29.

Retallack GJ, Veevers JJ and Morante R (1996) Global coal gap between Permian–Triassic extinction and Middle Triassic recovery of peat-forming plants. *Geological Society of America Bulletin* **108**, 195–207.

Romano C, Goudemand N, Vennemann TW, Ware D, Schneebeli-Hermann E, Hochuli PA, Bruhwiler T, Brinkmann W and Bucher H (2013) Climatic and biotic upheavals following the end-Permian mass extinction. *Nature Geoscience* **6**, 57–60.

Romano C, Jenks JF, Jattiot R, Scheyer TM, Bylund KG and Bucher H (2017) Marine Early Triassic Actinopterygii from Elko County (Nevada, USA): implications for the Smithian equatorial vertebrate eclipse. *Journal of Paleontology* **91**, 1025–46.

Saito R, Kaiho K, Oba M, Takahashi S, Chen ZQ and Tong JN (2013) A terrestrial vegetation turnover in the middle of the Early Triassic. *Global and Planetary Change* **105**, 152–9.

Schneebeli-Hermann E, Hochuli PA and Bucher H (2017) Palynofloral associations before and after the Permian–Triassic mass extinction, Kap Stosch, East Greenland. *Global and Planetary Change* **155**, 178–95.

Schneebeli-Hermann E, Hochuli PA, Bucher H, Goudemand N, Bruhwiler T and Galfetti T (2012) Palynology of the Lower Triassic succession of Tulong, South Tibet – evidence for early recovery of gymnosperms. *Palaeogeography, Palaeoclimatology, Palaeoecology* **339**, 12–24.

Schneebeli-Hermann E, Kürschner WM, Kerp H, Bomfleur B, Hochuli PA, Bucher H, Ware D and Roohi G (2015) Vegetation history across the Permian–Triassic boundary in Pakistan (Amb section, Salt Range). *Gondwana Research* **27**, 911–24.

Schulz E (1964) Sporen und pollen aus dem Mittleren Buntsandstein des germanischen Beckens. *Monatsberichte der deutschen Akademie der Wissenschaften* **6**, 597–606.

Segroves KL (1970) Permian spores and pollen from the Perth Basin, Western Australia. *Grana* **10**, 43–73.

Shigeta Y, Zakharov YD, Maeda H and Popov AM (2009) *The Lower Triassic System in the Abrek Bay Area, South Primorye, Russia*. Tokyo: National Museum of Nature and Science.

Stanley SM (2009) Evidence from ammonoids and conodonts for multiple Early Triassic mass extinctions. *Proceedings of the National Academy of Sciences of the United States of America* **106**, 15264–67.

Sun YD, Joachimski MM, Wignall PB, Yan CB, Chen YL, Jiang HS, Wang LN and Lai XL (2012) Lethally hot temperatures during the early Triassic Greenhouse. *Science* **338**, 366–70.

Sun YD, Wignall PB, Joachimski MM, Bond DPG, Grasby SE, Sun S, Yan CB, Wang LN, Chen YL and Lai XL (2015) High amplitude redox changes in the late Early Triassic of South China and the Smithian–Spathian extinction. *Palaeogeography, Palaeoclimatology, Palaeoecology* **427**, 62–78.

Thomazo C, Brayard A, Elmeknassi S, Vennin E, Olivier N, Caravaca G, Escarguel G, Fara E, Bylund KG, Jenks JF, Stephen DA, Killingsworth B, Sansjofre P and Cartigny P (2019) Multiple sulfur isotope signals associated with the late Smithian event and the Smithian/Spathian boundary. *Earth-Science Reviews*, published online 2 July 2018. doi: 10.1016/j.earscirev.2018.06.019.

Tong JA, Zuo JX and Chen ZQ (2007) Early Triassic carbon isotope excursions from South China: proxies for devastation and restoration of marine ecosystems following the end-Permian mass extinction. *Geological Journal* **42**, 371–89.

Tozer ET (1994) Canadian Triassic ammonoid faunas. *Geological Survey of Canada Bulletin* **467**, 1–663.

Van der Zwan CJ and Spaak P (1992) Lower to Middle Triassic sequence stratigraphy and climatology of the Netherlands, a model. *Palaeogeography, Palaeoclimatology, Palaeoecology* **91**, 277–90.

VanBuren R, Wai CM, Ou S, Pardo J, Bryant D, Jiang N, Mockler TC, Edger P and Michael TP (2018) Extreme haplotype variation in the desiccation-tolerant clubmoss *Selaginella lepidophylla*. *Nature Communications* **9**, 13.

Vigran JO, Bugge T, Mangerud G, Weitschat W and Mørk A (1998) Biostratigraphy and sequence stratigraphy of the Lower and Middle Triassic deposits from the Svalis Dome, Central Barents Sea, Norway. *Palynology* **22**, 89–141.

Vigran JO, Mangerud G, Mørk A, Worsley D and Hochuli PA (2014) Palynology and geology of the Triassic succession of Svalbard and the Barents Sea. *Geological Survey of Norway Special Publication* **14**, 1–247.

Visscher H (1974) The impact of palynology on Permian and Triassic stratigraphy in Western Europe. *Review of Palaeobotany and Palynology* **17**, 5–19.

Wignall PB, Bond DPG, Sun YD, Grasby SE, Beauchamp B, Joachimski MM and Blomeier DPG (2016) Ultra-shallow-marine anoxia in an Early Triassic shallow-marine clastic ramp (Spitsbergen) and the suppression of benthic radiation. *Geological Magazine* **153**, 316–31.

Zhang L, Zhao L, Chen ZQ, Algeo TJ, Li Y and Cao L (2015) Amelioration of marine environments at the Smithian–Spathian boundary, Early Triassic. *Biogeosciences* **12**, 1597–613.